Dissociation of Multisubunit Protein-Ligand Complexes in the Gas Phase

Evidence for Ligand Migration

Yixuan Zhang, Lu Deng, Elena N. Kitova, and John S. Klassen

Department of Chemistry and Alberta Glycomics Centre, University of Alberta,

Edmonton, Alberta, Canada T6G 2G2

Abstract

The results of collision-induced dissociation (CID) experiments performed on gaseous protonated and deprotonated ions of complexes of cholera toxin B subunit homopentamer (CTB_5) with the pentasaccharide (β-D-Gal$p$-(1→3)-β-D-Gal$p$NAc-(1→4)[α-D-Neu5Ac-(2→3)]-β-D-Gal$p$-(1→4)-β-D-Glc$p$ (GM1)) and corresponding glycosphingolipid (β-D-Gal$p$-(1→3)-β-D-Gal$p$NAc-(1→4)[α-D-Neu5Ac-(2→3)]-β-D-Gal$p$-(1→4)-β-D-Glc$p$-Cer (GM1-Cer)) ligands, and the homotetramer streptavidin (S_4) with biotin (B) and 1,2-dipalmitoyl-sn-glycero-3-phosphoethanolamine-N-(biotinyl) (Btl), are reported. The protonated $(CTB_5 + 5GM1)^{n+}$ ions dissociated predominantly by the loss of a single subunit, with the concomitant migration of ligand to another subunit. The simultaneous loss of ligand and subunit was observed as a minor pathway. In contrast, the deprotonated $(CTB_5 + 5GM1)^{n-}$ ions dissociated preferentially by the loss of deprotonated ligand; the loss of ligand-bound and ligand-free subunit were minor pathways. The presence of ceramide (Cer) promoted ligand migration and the loss of subunit. The main dissociation pathway for the protonated and deprotonated $(S_4 + 4B)^{n+/-}$ ions, as well as for deprotonated $(S_4 + 4Btl)^{n-}$ ions, was loss of the ligand. However, subunit loss from the $(S_4 + 4B)^{n+}$ ions was observed as a minor pathway. The $(S_4 + 4Btl)^{n+}$ ions dissociated predominantly by the loss of free and ligand-bound subunit. The charge state of the complex and the collision energy were found to have little effect on the relative contribution of the different dissociation channels. Thermally-driven ligand migration between subunits was captured in the results of molecular dynamics simulations performed on protonated $(CTB_5 + 5GM1)^{15+}$ ions (with a range of charge configurations) at 800 K. Notably, the migration pathway was found to be highly dependent on the

charge configuration of the ion. The main conclusion of this study is that the dissociation pathways of multisubunit protein-ligand complexes in the gas phase depend, not only on the native topology of the complex, but also on structural changes that occur upon collisional activation.

Introduction

Investigations into the assembly and organization of proteins into complexes and their interactions with other biomolecules (e.g. DNA, RNA, peptides, carbohydrates) and small molecules are stimulated by the critical importance of protein complexes and multiprotein assemblies in cellular processes [1-3]. There are a variety of experimental techniques available to probe the structures of protein complexes. High resolution structural data have been generated using X-ray crystallography and solution and solid state nuclear magnetic resonance spectroscopy [4,5]. A number of other experimental (e.g. electron microscopy, small angle scattering, circular dichroism) and computational methods can provide complementary structural information on protein complexes [6-9].

In recent years electrospray ionization mass spectrometry (ESI-MS) has emerged as an important tool for characterizing the composition and structure of multiprotein and protein-ligand complexes *in vitro* and, in some instances, it can provide insights into topology and connectivity and the identity and location of bound ligands [10-35]. The disruption of the non-covalent interactions within multiprotein complexes, either in solution or the gas phase, followed by the MS analysis of the monomeric/multimeric products can provide information about composition. The dissociation/disassembly of multiprotein complexes in solution can be achieved by altering the solution pH, temperature or ionic strength [15,16]. In the gas phase, energetic collisions with neutral gases (collision-induced dissociation, CID) are commonly used to cause the dissociation of multiply charged ions of intact protein complexes [16,17]. The use of CID, as well as other slow heating methods, such as infrared radiative multiphoton dissociation (IRMPD) [18] and blackbody infrared radiative dissociation (BIRD) [19-21], to establish the composition of multiprotein complexes is somewhat limited by the tendency of the

complexes to dissociate by the loss of a single, highly charged subunit, with the remaining complex resisting further dissociation. This phenomenon is believed to involve the asymmetric unfolding of the leaving subunit (relative to the other subunits in the complex); unfolding enhances the gas phase acidity/basicity of the subunit and promotes charge transfer [22-24]. In contrast, nearly complete disassembly of multiprotein complexes into monomers can be achieved with surface induced dissociation (SID), for which heating occurs on a much shorter timescale [25,26]. In addition to composition, MS combined with gas-phase activation methods such as CID can be used to probe the spatial arrangement of proteins within multiprotein complexes [27-30]. For example, it has been shown that subunits located on the periphery of the large multiprotein assemblies of the intact ribosome [27], RNA polymerase [28], 19S proteasome lid [29] and human eukaryotic initiation factor 3 protein complex [30] are preferentially lost upon collisional activation.

To date, there have been relatively few studies of the gas-phase dissociation of ligand-bound multiprotein/multisubunit complexes [31-35] and it remains unclear to what extent the location and nature of ligand binding can be probed in the gas phase. CID performed on the fully ligand-bound 24-mer of tryptophan RNA-binding attenuation protein (TRAP) resulted in the loss of the TRAP monomer, as well as the successive loss of ligands (Trp) [31]. Based on differences in the relative stabilities of the bound ligands, an asymmetric structure of the $TRAP_{24}$ assembly bound to 22 Trp molecules was suggested [31]. The results of both CID and SID of the heterotetrameric hemoglobin complex have been reported. SID resulted predominantly in the formation of α and β subunits, free of heme [32]. In contrast, CID proceeded by multiple pathways involving the loss of α and β subunits, heme, heme dimer and α and β subunits bound to heme [33],

5

Surprisingly, CID also produced $\alpha\beta_2$ trimers bound to four heme groups [32,33]. The loss of an α subunit, in its apo-form, from the intact holo-tetramer necessarily requires the migration of a heme group from one subunit to another. The process of ligand migration is, presumably, induced by collisional activation of the gaseous complex.

In the present study, the possibility of ligand migration within multisubunit protein complexes in the gas phase is examined in more detail. To this end, CID was performed on the complexes of two different multisubunit proteins, cholera toxin B subunit homopentamer (CTB$_5$) bound to its native ganglioside receptor β-D-Gal$p$-(1→3)-β-D-Gal$p$NAc-(1→4)[α-D-Neu5Ac-(2→3)]-β-D-Gal$p$-(1→4)-β-D-Glc$p$-Cer (GM1-Cer) and the soluble pentasaccharide β-D-Gal$p$-(1→3)-β-D-Gal$p$NAc-(1→4)[α-D-Neu5Ac-(2→3)]-β-D-Gal$p$-(1→4)-β-D-Glc$p$ (GM1) and the homotetramer streptavidin (S$_4$) with its high affinity ligand biotin (B) and biotin bound to a phosphatidylethanolamine group (PE), 1,2-dipalmitoyl-sn-glycero-3-phosphoethanolamine-N-(biotinyl) (Btl) (Figure S1). CTB$_5$ possesses five identical binding sites for GM1 (and GM1-Cer) and the intrinsic affinity (K$_a$) is reported to be between 10^5 and 10^7 M^{-1} [36-38]. According to the crystal structure of the the (CTB$_5$ + 5GM1) complex (PDB id 3CHB), the GM1 binding site is made up primarily from a single B subunit, with 18 direct or solvent mediated H-bonds between GM1 and amino acid residues located within the subunit and one H-bond with residue Gly33 from an adjacent subunit [39]. The S$_4$ homotetramer possesses four identical binding sites for B and the streptavidin-biotin interaction (K$_a \approx 10^{14}$ M^{-1}) is one of the strongest known [40]. Each B is stabilized primarily through intermolecular H-bonds and van-der-Waals interactions within a single subunit. Additionally, there is a contact between B and the aromatic ring of the Trp120 in an adjacent subunit [41]. CID

was performed on the protonated and deprotonated ions of the (CTB$_5$ + 5GM1), (CTB$_5$ + 5GM1-Cer), (S$_4$ + 4B) and (S$_4$ + 4Btl) complexes. The influence of charge state and collision energy on the dissociation pathways was assessed. Molecular dynamics (MD) simulations were performed on the protonated (CTB$_5$ + 5GM1)$^{15+}$ and deprotonated (CTB$_5$ + 5GM1)$^{14-}$ ions in an effort to elucidate the molecular details of the ligand migration and dissociation reactions.

Experimental

Proteins and ligands

The pentasaccharide β-D-Gal$p$-(1→3)-β-D-Gal$p$NAc-(1→4)[α-D-Neu5Ac-(2→3)]-β-D-Gal$p$-(1→4)-β-D-Glc$p$ (GM1, MW 998.34 Da), was obtained from Elicityl (Crolles, France) and bovine monosialotetrahexosylganglioside β-D-Gal$p$-(1→3)-β-D-Gal$p$NAc-(1→4)[α-D-Neu5Ac-(2→3)]-β-D-Gal$p$-(1→4)-β-D-Glc$p$-Cer (GM1-Cer) was purchased from Axxora LLC (San Diego, CA). The GM1-Cer sample was composed predominantly of two isoforms, d18:1-18:0 (MW 1545.88 Da) and d20:1-18:0 (MW 1573.91 Da). 1,2-dipalmitoyl-sn-glycero-3-phosphoethanolamine-N-(biotinyl) (Btl, MW 917.59 Da) and 1,2-dimyristoyl-sn-glycero-3-phosphocholine (DMPC, MW 677.50 Da) were purchased from Avanti Polar Lipids (Alabaster, AL). Recombinant membrane scaffold protein MSP1E1 (MW 27 494 Da), used in the preparation of nanodiscs (ND), was produced using plasmid pMSP1E1 acquired from Addgene (Cambridge, MA). Protein expression and purification was carried out using the procedure described at http://sligarlab.life.uiuc.edu/nanodisc.html. Cholera toxin B subunit (CTB, monomer MW 11 604 Da) and biotin (B, MW 244.09 Da) were purchased from Sigma-Aldrich Canada (Oakville, Canada). A recombinant, truncated form (containing residues 13-139)

of wild type streptavidin (S, monomer MW 13 271 Da) was used in this study; the plasmid was a gift from Prof. Stayton (University of Washington). The protein was expressed in *E. coli* and purified using procedures described elsewhere [42]. The solutions of S_4 and CTB_5 were exchanged into 200 mM aqueous ammonium acetate using an Amicon microconcentrator with a MW cut-off of 10 kDa, concentrated to 100 µM and stored at -20 °C and 4 °C, respectively, until needed.

Nanodiscs

NDs composed of DMPC and GM1-Cer or Btl were prepared using procedures reported elsewhere [43,44] and only brief description is given here. DMPC (in chloroform) was mixed with either GM1-Cer or Btl (in a 2:1 chloroform-methanol solution) at a 12:1 ratio; the solvent was removed under a gentle stream of nitrogen and replaced with Tris buffer containing 25 mM sodium cholate. MSP1E1 at a concentration of 0.3 to 0.4 mM was added to the cholate-solubilized lipid and GM1-Cer or Btl mixture at the desired ratios. After 30 min incubation at 23 ℃, the self-assembly process was initiated by adding an equal volume of pre-washed biobeads SM-2 (Bio-Rad), followed by gentle agitation for 4 h at 23 ℃. The beads were removed by sedimentation and the supernatant was then loaded onto a Superdex 200 HR 10/300 GL column (GE Healthcare). GM1-Cer-ND or Btl-ND fractions were collected, concentrated and dialyzed against 200 mM ammonium acetate (pH 7.0) using an Amicon microconcentrator with a MW cut-off of 30 kDa, then stored at -80 ℃. The concentration of the ND solutions was determined by absorbance at 280 nm using the extinction coefficient of MSP1E1.

Mass Spectrometry

All experiments were carried out using a Synapt G2-S quadrupole-ion mobility separation-time-of-flight (Q-IMS-TOF) mass spectrometer (Waters, UK), equipped with

a nanoflow ESI (nanoESI) source. To perform nanoESI, tips were produced from borosilicate capillaries (1.0 mm o.d., 0.68 mm i.d.) and pulled to ~5 μm using a P-97 micropipette puller (Sutter Instruments, Novato, CA). A platinum wire was inserted into the nESI tip, and a capillary voltage of 1.0−1.2 kV was applied to carry out nanoESI. Given below are representative instrumental conditions used in positive ion mode. A cone voltage of 35-50 V was used, and the source block temperature was maintained at 60 °C. The Trap and Transfer collision energies were maintained at 5 V and 2 V, respectively, for detection of the complexes. For the energy-resolved CID experiments, ions of interest were isolated using the quadrupole mass filter and then subjected to CID by increasing the collision energy in the Trap ion guide from 10 to 120 V for the $(CTB_5 + 5GM1)^{n+}$ and $(CTB_5 + 5GM1\text{-}Cer)^{n+}$ ions or from 3 to 70 V for the $(S_4 + 4B)^{n+}$ and $(S_4 + 4Btl)^{n+}$ ions, using steps of 2 or 3 V. Argon was used in the Trap and Transfer ion guides at a pressure of 1.42×10^{-2} mbar and 1.74×10^{-2} mbar, respectively. Helium, at a flow rate of 151 mL min^{-1}, was introduced into the He chamber preceding the traveling wave ion mobility (TWIMS) device. Data acquisition and processing were carried out using MassLynx (v 4.1).

To produce gaseous ions of the protein complexes containing the water soluble ligands (GM1 or B), nanoESI was performed on aqueous 200 mM ammonium acetate solutions containing 6 μM of CTB_5 and 38 μM GM1, or 5 μM S_4 and 20 μM B. To produce gaseous ions of the protein complexes containing the insoluble GM1-Cer or Btl ligands, nanoESI was performed on aqueous 200 mM ammonium acetate solutions containing 6 μM of CTB_5 and 10 μM ND with 8% GM1-Cer or 5 μM S_4 and 10 μM ND with 8% Btl. Mild in-source dissociation was used to release the $(CTB_5 + 5GM1\text{-}Cer)^{n+/-}$ and $(S_4 + 4Btl)^{n+/-}$ ions from the gaseous ND complexes [45]. Shown in Figures S2 and

S3 are representative mass spectra measured in positive and negative ion mode, respectively.

The average charge states (*ACS*) of the subunit product ions (i.e. $CTB^{x+/-}$ and $S^{x+/-}$) were calculated from the CID mass spectra using eq 1:

$$ACS = \frac{\sum_{x} xAb_x}{\sum_{x} Ab_x} \qquad (1)$$

where Ab_x and x are the relative abundance and the charge state of each $CTB^{x+/-}$ or $S^{x+/-}$ ion. The *ACS* values of the $(CTB + GM1)^{y+/-}$, $(CTB + GM1-Cer)^{y+/-}$ and $(S+Btl)^{y+/-}$ product ions were calculated in a similar manner.

Computational Methods

MD simulations were performed using the Amber 11 program suite [46] (Accelrys, San Diego, CA). Currently with Amber atomic charges and atom type parameters are available only for the charged forms of the Arg, N-terminal Thr (NThr) and C-terminal Asn (CAsn) residues. Consequently, it was necessary to develop charges and parameters for the neutral form of Arg, NThr and CAsn. The charges and parameters for the neutral form of Arg were established in a previous study [47]. The charges for the neutral form of NThr and CAsn, incorporated into dipeptides (NThr-Gly-NME and ACE-Gly-CAsn, respectively), were parameterized using the RESP ESP Charge Derive server [48,49] and Gaussian C.01 [50], enforcing net neutrality across the residues. The crystal structure of the CTB_5 subunit complexed with five GM1 (PDB ID: 3CHB) has been reported [51]. The initial geometry of the CTB_5 was generated by converting all of the charged acidic and basic amino acid residues to their neutral forms. Incomplete GM1 structures found in the crystal structure were corrected by aligning each incomplete ligand to the complete

ligand structure and grafting the missing atoms onto each ligand using Open Babel 2.0 [52,53].

The $(CTB_5 + 5GM1)$ complex at charge states +15 and -14 were chosen for investigation. For the $(CTB_5 + 5GM1)^{15+}$ ion, only the basic residues (Lys, Arg and His) on the surface of CTB_5 (<5 Å from the surface) and N-Thr were considered as possible protonation sites [54]. To mimic the dissociation pathways observed in the CID experiments, seven of the fifteen charges were placed on subunit D and the other eight were distributed evenly on other four subunits (E, F, G, H). The twelve different charge configurations considered are listed in Table S1. Topology and coordinate files for the simulations of each charge configuration were created using the Antechamber module of the AmberTools (version 11) [55]. To reflect the observed dissociation pathways, all five GM1 ligands of the $(CTB_5 + 5GM1)^{14-}$ ion were deprotonated (at the sialic acid residue); the other nine charges were distributed asymmetrically among the five subunits (five charges on subunit D and one charge on each of the other four subunits). Only Glu and Asp residues on the surface of CTB_5 (<5 Å from the surface) were considered as possible deprotonation sites (Table S1). The MD simulations were performed using the Amber 03 force field [56] for CTB_5 and a general Amber force field (GAFF) [57] for GM1. The MD integration time step was 1 fs; bonds involving hydrogen atoms were constrained with SHAKE. Following 1000 steps of minimization, the system was heated from 300K to 800 K within 20,000 steps (0.02 ns). The temperature was then held constant at 800 K and 3 ns of dynamics were performed. Trajectory analysis and the calculation of the radius of gyration (Rg) were performed using the Visual Molecular Dynamics package [58].

Results and discussion

a. CID of $(CTB_5 + 5GM1)^{n+/-}$ and $(CTB_5 + 5GM1\text{-}Cer)^{n+/-}$ ions

Representative nanoESI mass spectra acquired in both positive and negative ion mode for an aqueous ammonium acetate (200 mM) solution of CTB_5 (6 μM) and GM1 (38 μM) are shown in Figure 1. The major protein ions detected correspond to protonated (+ mode) or deprotonated (- mode) homopentamer bound to three, four or five GM1 ligands, i.e., $(CTB_5 + iGM1)^{n+}$ ions where i = 3, 4 and 5, at charge states +13, +14, +15 (Figure 1a) and $(CTB_5 + iGM1)^{n-}$ ions where i = 3, 4 and 5, at charge states -12, -13, -14 (Figure 1b). Control nanoESI-MS measurements, employing the reference protein method [59], were performed in order to confirm that observed ions were formed from the specific $(CTB_5 + iGM1)$ complexes in solution, with no contribution from nonspecific ligand binding during the ESI process (data not shown) [60]. Energy-resolved CID of the protonated $(CTB_5 + 5GM1)^{n+}$ ions, at charge states +14 and +15, and deprotonated $(CTB_5 + 5GM1)^{n-}$ ions, at charge states -12, -13 and -14, was carried out as described in the Experimental section. A summary of the dissociation pathways observed for the $(CTB_5 + 5GM1)^{n+}$ and $(CTB_5 + 5GM1)^{n-}$ ions is given in Scheme 1.

Shown in Figure 2 and 3 are representative CID mass spectra acquired for the $(CTB_5 + 5GM1)^{14+}$ and $(CTB_5 + 5GM1)^{14-}$ ions, respectively; CID mass spectra measured for the $(CTB_5 + 5GM1)^{15+}$, $(CTB_5 + 5GM1)^{13-}$ and $(CTB_5 + 5GM1)^{12-}$ ions are shown in Figures S4 - S6. At all collision energies investigated, the major dissociation pathway observed for the protonated $(CTB_5 + 5GM1)^{n+}$ ions was the loss of a single subunit, i.e., CTB^{x+}, where x = 4 − 6 (for +14 parent ion) and x = 4 − 7 (+15) and the formation of the complementary $(CTB_4 + 5GM1)^{(n-x)+}$ ions, where (n-x) = 8 − 10 (+14)

12

and (n-x) = 8 − 11 (+15). The *ACS* (Table 1) of the CTB^{x+} product ions (5.3 ± 0.1 for +14 and 5.9 ± 0.1 for +15) was found to be independent of collision energy. A second (minor) pathway, observed at higher collision energies (>40 V), was the simultaneous loss of CTB subunit and GM1, i.e., $(CTB + GM1)^{y+}$ ions, where y = 4 and 5 (for +14) and y = 5 and 6 (for +15), and the formation of the complementary $(CTB_4 + 4GM1)^{10+}$ and $(CTB_4 + 4GM1)^{9+}$ ions. Notably, the loss of GM1 (charged or neutral) was not observed at any collision energy.

The dominant dissociation pathway observed for the $(CTB_5 + 5GM1)^{n-}$ ions, at charge states -12, -13 and -14, (Figures S6 and S5 and Figure 3) was the sequential loss of the deprotonated GM1, leading to abundant $(CTB_5 + iGM1)^{[n-(5-i)]-}$ product ions, where $i = 0 − 4$. Subunit loss, which resulted in CTB^{x-} ions (*ACS* of 4.8 ± 0.1 (for -12), 4.9 ± 0.1 (-13) and 5.2 ± 0.1 (-14), Table 1) and the complementary $(CTB_4 + 5GM1)^{(n-x)-}$ ions, was a minor pathway. The collision energy was found to have little influence on the CID mass spectra, although a second minor pathway, involving the loss of $(CTB + GM1)^{5-}$ and $(CTB + GM1)^{6-}$ ions, was observed for charge states -13 and -14 at higher collision energies (Figure S5 and Figure 3).

The native receptor of CTB_5 is the ganglioside GM1-Cer, which possesses ceramide at the reducing end of the pentasaccharide [61]. To assess whether the presence of ceramide influences the dissociation pathways, CID was performed on $(CTB_5 + 5GM1-Cer)^{n+}$ ions at charge states +14, +15 and +16, and $(CTB_5 + 5GM1-Cer)^{n-}$ ions at charge states -13, -14, and -15. Representative CID spectra for the $(CTB_5 + 5GM1-Cer)^{14+}$ and $(CTB_5 + 5GM1-Cer)^{14-}$ ions are shown in Figure 4 and Figure 5, respectively. CID mass spectra for the other charge states investigated are shown in Figures S7 - S10. Dissociation of the $(CTB_5 + 5GM1-Cer)^{n+}$ ions proceeded by the loss of a single CTB

subunit and by the simultaneous loss of CTB subunit and GM1-Cer. This is similar to what was observed for the $(CTB_5 + 5GM1)^{n+}$ ions. However, the presence of ceramide measurably enhanced (by ~6%) the latter pathway. The *ACS* of the ejected subunit (5.2 ± 0.1 (+14), 5.9 ± 0.1 (+15) and 6.5 ± 0.1 (+16) are similar to those of the $(CTB + GM1-Cer)^{y+}$ product ions and those of subunits ejected from CTB_5^{n+} ions (Table 1). CID of $(CTB_5 + 5GM1-Cer)^{n-}$ ions proceeded by two major pathways, the loss of deprotonated GM1-Cer and the loss of subunit. The enhancement of the subunit loss pathway (compared to that for the corresponding $(CTB_5 + 5GM1)^{n-}$ ions) was particularly significant for the -13 charge state (Figure S9). The *ACS* of the ejected subunits (4.8 ± 0.1 (-13), 5.0 ± 0.1 (-14), and 5.4 ± 0.2 (-15)) are similar to those found for the corresponding $(CTB_5 + 5GM1)^{n-}$ ions (Table 1).

The CID results obtained for protonated and deprotonated ions of the $(CTB_5 + 5GM1)$ and $(CTB_5 + 5GM1-Cer)$ complexes are intriguing. The loss of a single subunit, free of ligand, necessarily requires that the ligand originally bound to the ejected subunit migrate to another subunit. The migration process is, presumably, induced upon collisional heating of the gaseous complex. It is also possible that migration occurs prior to CID (i.e., during or after desolvation the complex). However, this possibility is viewed as unlikely given that the intermolecular interactions in a number of protein-ligand complexes have been shown to be preserved upon transfer of the complexes from solution to the gas phase [47,62-67]. The observation of ligand migration between subunits is, perhaps, a surprising finding given that it is generally accepted that the loss of a charge-enriched subunit requires unfolding [22-24,34,68-70]. Subunit unfolding would, in turn, be expected to result in the loss of intermolecular protein-ligand interactions and, consequently, the loss of the ligand from the complex. However, for the protonated

complexes, GM1 loss is not observed under any conditions. The absence of this pathway would seem to suggest a high kinetic barrier to the cleavage of the intermolecular interactions. However, these same interactions are necessarily lost during the migration process (to a neighbouring subunit). While the exact mechanism(s) of ligand migration cannot be established from the CID results alone, the experimental observations can be reasonably explained in terms of a multistep mechanism involving sequential intermolecular bond cleavage and formation. According to this view, the energetic penalty associated with the cleavage of the intermolecular interactions (presumably H-bonds) with the subunit to which the ligand was originally bound is offset by the formation of new interactions with one or more of the other subunits. Moreover, that the presence of ceramide enhances ligand migration for the $(CTB_5 + 5GM1\text{-}Cer)^{n-}$ ions suggests that the long acyl chains of the ceramide moiety aid in the migration process through the formation of nonspecific, nonpolar interactions with the subunits. The suggestion is supported by the results of recent studies of the dissociation kinetics of gaseous complexes of bovine β-lactoglobulin and long chain fatty acids, which revealed the gaseous complexes are stabilized predominantly by protein-lipid interactions [64, 67,71].

Equally intriguing is the observation of the simultaneous loss of a subunit bound to GM1. On its own, this finding would seem to suggest that ligand binding does not necessarily preclude subunit unfolding. Some insight into the degree of subunit unfolding can be gleaned from the *ACS* measured for the ejected subunits and subunit-ligand complexes from the $(CTB_5 + 5GM1)^{n+}$, $(CTB_5 + 5GM1\text{-}Cer)^{n+}$ ions (Table 1). For the protonated ions, it can be seen that the charge states of the $(CTB + GM1)^{y+}$ and $(CTB + GM1\text{-}Cer)^{y+}$ product ions are similar to those of the corresponding CTB^{x+} ions produced

from the same reactant ion. Assuming that the *ACS* of the leaving subunit correlates with its surface area [22-24], these results suggest that ligand binding does not preclude unfolding.

That the deprotonated $(CTB_5 + 5GM1)^{n-}$ ions dissociate preferentially by the loss of deprotonated GM1, as opposed to subunit ejection, can be explained in terms of the relatively low gas phase acidities of carbohydrates and their ability to effectively compete with the protein for charge [63,72] and the influence of Coulombic repulsion on the dissociation kinetics. As discussed elsewhere [22,34,73], Coulombic repulsion between charged product ions produced from gaseous non-covalent protein complexes will lead to a reduction in the dissociation activation energy (E_a). Consequently, the E_a for the loss of deprotonated GM1 is expected to be significantly lower than for the loss of neutral GM1 and, presumably, lower than for GM1 migration to another subunit.

b. CID of $(S_4 + 4B)^{n+/-}$ and $(S_4 + 4Btl)^{n+/-}$ ions

The CID results obtained for the $(CTB_5 + 5GM1)^{n+/-}$ and $(CTB_5 + 5GM1-Cer)^{n+/-}$ ions provide evidence for the occurrence of ligand migration between subunits upon collisional activation. To test whether the phenomenon of ligand migration is general for multisubunit protein-ligand complexes in the gas phase, CID measurements were extended to the $(S_4 + 4B)^{n+/-}$ and $(S_4 + 4Btl)^{n+/-}$ ions. Shown in Figure S11 are nanoESI mass spectra acquired in both positive and negative ion mode for an aqueous ammonium acetate (200 mM) solution of S_4 (5 μM) and B (20 μM). The most abundant protein ions detected corresponded to protonated or deprotonated homotetramer bound to four B molecules, i.e., $(S_4 + 4B)^{n+}$ at charge states +15 and +16 (Figure S11a) and $(S_4 + 4B)^{n-}$ ions at charge states -12, -13 and -14 (Figure S11b). Representative CID mass spectra obtained for the $(S_4 + 4B)^{15+}$ and $(S_4 + 4B)^{16+}$ ions are shown in Figure S12 and Figure

S13. The major dissociation pathway was the loss of B, either in its protonated or neutral forms. The loss of a single subunit, i.e., S^{x+}, with an *ACS* of x = 6.8 ± 0.1 (+15) and 6.9 ± 0.1 (+16), was observed as a minor pathway (Table S2); this pathway was enhanced at higher collision energies. Because substantial loss of B was observed under the CID conditions used, it is not possible to conclude whether ligand migration take place prior to subunit ejection based solely on the appearance of S^{x+} ions. However, within a narrow range of collision energies (26-30V for +15 and 12 - 30 V for +16), $(S_3 + 4B)^{(n-x)+}$ ions could be detected, although at low abundance. These results confirm that collisional activation does promote ligand migration between subunits.

Representative CID mass spectra of the $(S_4 + 4Btl)^{15+}$ and $(S_4 + 4Btl)^{16+}$ ions are shown in Figures S14 and S15, respectively. Interestingly, the loss of a subunit (*ACS* of the S^{x+} product ions are 7.1 ± 0.1 for +15 and 7.3 ± 0.1 for +16, Table S2) was the major dissociation pathway observed at all collision energies investigated (this pathway is enhanced by 85% compared to the same pathway involving $(S_4 + 4B)^{n+}$); no ligand loss was detected. These results indicate that PE, much like does ceramide, promotes ligand migration between subunits, presumably through the formation of nonspecific intermolecular interactions. A minor pathway involving the loss of $(S + Btl)^{y+}$ ions, y = 6.8 ± 0.1 (+15) and 6.9 ± 0.1 (+16), was also identified. Curiously, the *ACS* of the S^{x+} product ions produced from the $(S_4 + 4Btl)^{n+}$ ions are somewhat larger than for S^{x+} ions produced from the corresponding $(S_4 + 4B)^{n+}$ ions (Table S2). On its own, this suggests that Btl migration promotes additional unfolding of the subunits. The reason for this effect is not clear.

For the deprotonated $(S_4 + 4B)^{n-}$ ions, at charge states -12 and -13, the sequential loss of B (in its neutral or deprotonated forms) was the only dissociation pathway

observed at all collision energies investigated (Figure S16 and Figure S17, respectively). Similar results were obtained for the $(S_4 + 4Btl)^{13-}$ and $(S_4 + 4Btl)^{12-}$ ions, whereby only the loss of deprotonated Btl was observed (Figure S18 and Figure S19, respectively).

c. MD simulations

The aforementioned CID results suggest that ligand migration can generally occur upon collision activation of multiprotein-ligand complexes in the gas phase. However, on their own, they do not provide any insight into the underlying mechanisms. With the goal of elucidating the influence of charge on the ligand migration and subunit loss processes, MD simulations were performed on twelve different charge configurations of the $(CTB_5 + 5GM1)^{15+}$ ion in which seven charges were located on subunit D and two charges placed on each of other four subunits, E, F, G and H (Table S1). The GM1 ligands were treated as neutrals in all cases.

The initial structure of the $(CTB_5 + 5GM1)^{15+}$ ion used for the simulations is shown in Figure S20a. Shown in Figure S20b are plots of Rg measured along the trajectory for each of the twelve charge configurations considered. A common feature is a gradual increase in the magnitude of Rg of the ion with simulation time. This observation indicates that the overall size of the complex is increasing with time due to thermally-induced unfolding of the subunits. Interestingly though, all of the subunits, not just subunit D, exhibited significant unfolding. Analysis of the trajectories also reveals that, in all cases, the original interactions between GM1 and the CTB subunits were altered and the nature of the changes was strongly dependent on charge configuration. For nine (B15_1, B15_2, B15_3, B15_4, B15_6, B15_7, B15_10, B15_11 and B15_12) of the twelve configurations considered, ligand migration to another subunit was observed. However, the "donor" and "acceptor" subunits varied depending on configuration. For

charge configuration B15_12, GM1 migrated from subunit D to E (Figure S20c), from H to D for B15_3 (Figure S20d) and B15_7 (Figure S20e), from G to H for B15_1 (Figure S20f) and B15_6 (Figure S20g), from E to D for B15_4 (Figure S20h), and from F to G for B15_11 (Figure S20i). Interestingly, migration of more than one ligand was also observed for B15_2 (Figure S20j) and B15_10 (Figure S20k). For B15_2, GM1 molecules migrated from E to D and from G to H. In charge configuration B15_10, GM1 molecules originally bound to F and G migrated so as to bridge both subunits, similarly GM1 molecules on subunits D and E migrated so as to bridge both subunits and GM1 from subunit H migrated to the interface of D and H. For the three remaining charge state configurations, ligand migration within a subunit was observed. A representative structure from charge configuration B15_9 (at 1.5 ns) is shown in Figure S20l. GM1 located on the subunit D migrated from the original binding site to the N-terminus where it was stabilized by two ionic hydrogen bonds between charged N-terminal Thr and the branching Gal residue.

Although the results of the MD simulations must be viewed with caution, due to their inherent limitations (simulation time (ns) is much shorter compared to CID timescale (μs), charges cannot move, and uncertainty related to the simulation temperature), they do suggest that the migration of GM1 within and between subunits readily occurs upon heating of protonated $(CTB_5 + 5GM1)^{15+}$. These findings are consistent with the tendency of the $(CTB_5 + 5GM1)^{n+}$ ions to dissociate by the loss of subunit or subunit-ligand complex. The MD results also suggest that the mechanism of ligand migration is highly dependent on the charge configuration.

For comparison purposes, MD simulations were also performed on the $(CTB_5 + 5GM1)^{14-}$ ion in which all five GM1 ligands were deprotonated (at the sialic acid residue);

the other nine charges were distributed asymmetrically among the five subunits (five

charges on subunit D and one charge on each of the other four subunits). Analysis of the

MD trajectory reveals the sequential loss of deprotonated GM1; no ligand migration to

other subunits was observed. These findings are consistent with the experimental

observations. Interestingly, deprotonated GM1 was lost preferentially from subunits E

and H, not from D; GM1 loss from D occurred only after the subunit underwent

significant unfolding. The structure shown in Figure S20m was calculated at 1.5 ns, after

the loss of four GM1 (initially on subunits D, E, F and H).

Conclusions

The results of CID measurements performed on the protonated and deprotonated ions of

the $(CTB_5 + 5GM1)$, $(CTB_5 + 5GM1-Cer)$, $(S_4 + 4B)$ and $(S_4 + 4Btl)$ complexes reveal

that multiple dissociation pathways are accessible to gaseous multisubunit protein-ligand

complexes upon collisional activation. The relative contribution of the three dissociation

pathways: (1) loss of the ligand-unbound protein subunit, (2) loss of subunit-ligand

complex and (3) loss of ligand (neutral or charged), appears to reflect the strength of

intermolecular protein-ligand interactions in gas phase. It is proposed that a high

energetic barrier to ligand loss promotes ligand migration to other subunits, as well as the

ejection of the ligand-subunit complex, upon collisional activation. The presence of

ceramide or PE groups, which can participate in nonspecific interactions with subunits,

enhances the loss of ligand-free and ligand-bound subunit. The results of MD simulations

performed on the $(CTB_5 + 5GM1)^{15+}$ ion with different charge configurations reveal that

ligands, when neutral, are highly mobile and readily migrate within and between subunits.

Moreover, the mechanism of ligand migration appears to be highly dependent on charge

configuration. In agreement with experiment, the loss of deprotonated ligand readily

occurred in MD simulations performed on the $(CTB_5 + 5GM1)^{14-}$ ion. Taken together, the results of this study suggest that collisional activation of multisubunit protein-ligand complexes in the gas phase is likely to induce significant changes to the nature of the protein-ligand interactions. Consequently, caution must be exercised when using MS and CID (or similar activation methods) to establish the location(s) of ligands bound to multiprotein complexes.

References

(1) Rual, J.F., Venkatesan, K., Hao, T., Hirozane-Kishikawa, T., Dricot, A., Li, N., Berriz, G.F., Gibbons, F.D., Dreze, M., Ayivi-Guedehoussou, N., Klitgord, N., Simon, C., Boxem, M., Milstein, S., Rosenberg, J., Goldberg, D.S., Zhang, L.V., Wong, S.L., Franklin, G., Li, S., Albala, J.S., Lim, J., Fraughton, C., Llamosas, E., Cevik, S., Bex, C., Lamesch, P., Sikorski, R.S., Vandenhaute, J., Zoghbi, H.Y., Smolyar, A., Bosak, S., Sequerra, R., Doucette-Stamm, L., Cusick, M.E., Hill, D.E., Roth, F.P., Vidal, M.: Towards a proteome scale map of the human protein-protein interaction network. *Nature* **437**, 1173−1178 (2005)

(2) Gavin, A.C, Aloy, P., Grandi, P., Krause, R., Boesche, M., Marzioch, M., Rau, C., Jensen, L.J., Bastuck, S., Dümpelfeld, B., Edelmann, A., Heurtier, M.A., Hoffman, V., Hoefert, C., Klein, K., Hudak, M., Michon, A.M., Schelder, M., Schirle, M., Remor, M., Rudi, T., Hooper, S., Bauer, A., Bouwmeester, T., Casari, G., Drewes, G., Neubauer, G., Rick, J.M., Kuster, B., Bork, P., Russell, R.B., Superti-Furga, G.: Proteome survey reveals modularity of the yeast cell machinery. *Nature* **440**, 631–636 (2006)

(3) Robinson, C.V., Sali, A., Baumeister, W.: The molecular sociology of the cell. *Nature* **450**, 973–982 (2007)

(4) Ilari, A., Savino, C.: Protein structure determination by x-ray crystallography. *Methods Mol. Biol*. **452**, 63-87 (2008)

(5) Nietlispach, D., Mott, H.R., Stott, K.M., Nielsen, P.R., Thiru, A., Laue, E.D.: Structure determination of protein complexes by NMR. *Methods Mol. Biol*. **278**, 255-288 (2004)

(6) Jonic, S., Vénien-Bryan, C.: Protein structure determination by electron cryo-microscopy. *Curr. Opin. Pharm*. **9**, 636–642 (2009)

(7) Mertens, H.D., Svergun, D.I.: Structural characterization of proteins and complexes using small-angle X-ray solution scattering. *J. Struct. Biol*. **172**, 128-141 (2010)

(8) Greenfield, N.J.: Using circular dichroism spectra to estimate protein secondary structure. *Nature Prot*. **1**, 2876 – 2890 (2007)

(9) Kelley, L.A., Sternberg, M.J.E.: Protein structure prediction on the Web: a case study using the Phyre server. *Nature Prot*. **4**, 363-371 (2009)

(10) Loo, J.A.: Electrospray ionization mass spectrometry: a technology for studying noncovalent macromolecular complexes. *Int. J. Mass Spectrom.* **200**, 175-186 (2000)

(11) Benesch, J.L.P., Robinson, C.V.: Mass spectrometry of macromolecular assemblies: preservation and dissociation. *Curr. Opin. Struct. Biol*. **16**, 245-251 (2006)

(12) Barrera, N.P., Robinson, C.V.: Advances in the mass spectrometry of membrane proteins: from individual proteins to intact complexes. *Annu. Rev. Biochem*. **80**, 247-271 (2011)

(13) Uetrecht, C., Heck, A.J.: Modern biomolecular mass spectrometry and its role in studying virus structure, dynamics, and assembly. *Angew. Chemie Int. Ed*. **50**, 8248–8262 (2011)

(14) van den Heuvel, R.H.H., Heck, A.J.R.: Native protein mass spectrometry: from intact oligomers to functional machineries. *Curr. Opin. Chem. Biol*. **8**, 519–526 (2004)

 (15) Hall, Z., Politis, A., Robinson, C.V.: Structural modeling of heteromeric protein complexes from disassembly pathways and ion mobility-mass spectrometry. *Structure* **20**, 1596–1609 (2012).

(16) Taverner, T., Hernández, H., Sharon, M., Ruotolo, B.T., Matak-Vinković, D., Devos, D., Russell, R.B., Robinson, C.V.: Subunit architecture of intact protein complexes from mass spectrometry and homology modeling. *Acc. Chem. Res*. **41**, 617-627 (2008)

(17) Benesch, J.L.P., Ruotolo, B.T., Simmons, D.A., Robinson, C.V.: Protein complexes in the gas phase: technology for structural genomics and proteomics. *Chem. Rev*. **107**, 3544-3567 (2007)

(18) McLafferty, F.W., Guan, Z.Q., Haupts, U., Wood, T.D., Kelleher, N.L.: Gaseous conformational structures of cytochrome c. *J. Am. Chem. Soc*. **120**, 4732–4740 (1998)

(19) Dunbar, R.C., McMahon, T.B.: Activation of unimolecular reactions by ambient black-body radiation. *Science* **279**, 194–197 (1997)

(20) Price, W.D., Schnier, P.D., Williams, E.R.: Tandem mass spectrometry of large biomolecule ions by blackbody infrared radiative dissociation. *Anal. Chem*. **68**, 859–866 (1996)

(21) Dunbar, R.C.: BIRD (blackbody infrared radiative dissociation): Evolution, principles, and applications. *Mass Spectrom. Rev*. **23**, 127– 158 (2004)

(22) Wanasundara, S.N., Thachuk, M.: Theoretical investigations of the dissociation of charged protein complexes in the gas phase. *J. Am. Soc. Mass Spectrom*. **18**, 2242–2253 (2007)

(23) Benesch. J.L., Aquilina, J.A., Ruotolo, B.T., Sobott, F., Robinson, C.V.: Tandem mass spectrometry reveals the quaternary organization of macromolecular assemblies. *Chem. Biol.* **13**, 597-605 (2006)

(24) Jurchen, J.C., Williams, E.R.: Origin of asymmetric charge partitioning in the dissociation of gas-phase protein homodimers. *J. Am. Chem. Soc*. **125**, 2817–2826 (2003)

(25) Jones, C.M., Beardsley, R.L., Galhena, A.S., Dagan, S., Cheng, G.L., Wysocki, V.H.: Symmetrical gas-phase dissociation of noncovalent protein complexes via surface collisions. *J. Am. Chem. Soc*. **128**, 15044–15045 (2006)

(26) Beardsley, R.L., Jones, C.M., Galhena, A.S., Wysocki, V.H., Blackwell, A.E., Dodds, E.D., Bandarian, V., Wysocki, V.H.: Revealing the quaternary structure of a heterogeneous noncovalent protein complex through surface-induced dissociation. *Anal. Chem*. **83**, 2862-2865 (2011)

(27) Rostom, A.A., Fucini, P., Benjamin, D.R., Juenemann, R., Nierhaus, K.H., Hartl, F.U., Dobson, C.M., Robinson, C.V.: Detection and selective dissociation of intact ribosomes in a mass spectrometer. *Proc. Natl Acad. Sci*. **97**, 5185-5190 (2000)

(28) Lorenzen, K., Vannini, A., Cramer, P., Heck, A.J.: Structural biology of RNA polymerase III: mass spectrometry elucidates subcomplex architecture. *Structure* **15** 1237-1245 (2007)

(29) Robinson, C.V., Deshaies, R.J., Sharon, M., Ambroggio, X.I., Taverner, T.: Structural organization of the 19S proteasome lid: insights from MS of intact complexes. *PLoS Biol*. **4**, e267 (2006).

(30) Damoc, E., Fraser, C.S., Zhou, M., Videler, H., Mayeur, G.L., Hershey, J.W., Doudn, J.A., Robinson, C.V., Leary, J.A.: Structural characterization of the human eukaryotic initiation factor 3 protein complex by mass spectrometry. *Mol. Cell Prot*. **6**, 1135-1146 (2007)

(31) McCammon, M.G., Hernández, H., Sobott, F., Robinson, C.V.: Tandem mass spectrometry defines the stoichiometry and quaternary structural arrangement of tryptophan molecules in the multiprotein complex TRAP. *J. Am. Chem. Soc*. **126**, 5950-5901 (2004)

(32) Beardsley, R.L., Jones, C.M., Galhena, A.S., Wysocki, V.H.: Noncovalent protein tetramers and pentamers with "n" charges yield monomers with n/4 and n/5 charges. *Anal Chem*. **4**, 1347-1356 (2009)

(33) Versluis, C., Heck, A.J.R.: Gas-phase dissociation of hemoglobin. *Int. J. Mass Spectrom.* **210-211**, 637-649 (2001)

(34) Felitsyn, N., Kitova, E.N., Klassen, J.S.: Thermal decomposition of a gaseous multiprotein complex studied by blackbody infrared radiative dissociation. Investigating the origin of the asymmetric dissociation behavior. *Anal. Chem.* **73**, 4647-4661 (2001)

(35) Hyung, S.J., Robinson, C.V., Ruotolo, B.T.: Gas-phase unfolding and disassembly reveals stability differences in ligand-bound multiprotein complexes. *Chem. Biol.* **16**, 382-390 (2009)

(36) Turnbull, W.B., Precious, B.L., Homans, S.W.: Dissecting the cholera toxin-ganglioside GM1 interaction by isothermal titration calorimetry. *J. Am. Chem. Soc.* **126**, 1047-1054 (2004)

(37) Lauer, S., Goldstein, B., Nolan, R.L., Nolan, J.P.: Analysis of cholera toxin-ganglioside interactions by flow cytometry. *Biochemistry* **41**, 1742-1751 (2002)

(38) Schafer, D.E., Thakur, A.K.: Quantitative description of the binding of GM1 oligosaccharide by cholera enterotoxin. *Cell Biophysica* **4**, 25-40 (1982).

(39) Merritt, E.A., Sarfaty, S., van den Akker, F., L'Hoir, C., Martial, J.A., Hol, W.G.: Crystal structure of cholera toxin B-pentamer bound to receptor GM1 pentasaccharide. *Prot. Sci.* **3**, 166-175 (1994)

(40) Chilkoti, A., Stayton, P.S.: Molecular origins of the slow streptavidin-biotin dissociation kinetics. *J. Am. Chem. Soc.* **117**, 10622-10628 (1995).

(41) Freitag, S., Le Trong, I., Klumb, L., Stayton, P.S., Stenkamp, R.E.: Structural studies of the streptavidin binding loop. *Prot. Sci.* **6**, 1157–1166 (1997)

(42) Chilkoti, A., Tan, P.H., Stayton, P.S.: Site-directed mutagenesis studies of the high-affinity streptavidin-biotin complex: contributions of tryptophan residues 79, 108, and 120. *Proc. Natl Acad. Sci*. **92**, 1754-1758 (1995)

(43) Ritchie, T.K., Grinkova, Y.V., Bayburt, T.H., Denisov, I.G., Zolnerciks, J.K., Atkins, W.M., Sligar, S.G.: Chapter 11. Reconstitution of membrane proteins in phospholipid bilayer nanodiscs. *Methods Enzymol*. **464**, 211-231 (2009)

(44) Bayburt, T.H., Grinkova, Y.V., Sligar, S.G.: Self-assembly of discoidal phospholipid bilayer nanoparticles with membrane scaffold proteins. *Nanoletters* **2**, 853-856 (2002)

(45) Zhang, Y., Liu, L., Daneshfar, R., Kitova, E.N., Li, C., Jia, F., Cairo, C.W., Klassen, J.S.: Protein-glycosphingolipid interactions revealed using catch-and-release mass spectrometry. *Anal. Chem*. **84**, 7618-7621 (2012)

(46) Case, D.A., Darden, T.A., Cheatham III, T.E., Simmerling, C.L., Wang, J., Duke, R.E., Luo, R., Walker, R.C., Zhang, W., Merz, K.M., Roberts, B., Wang, B., Hayik, S., Roitberg, A., Seabra, G., Kolossváry, I., Wong, K.F., Paesani, F., Vanicek, J., Liu, J., Wu, X., Brozell, S.R., Steinbrecher, T., Gohlke, H., Cai, Q., Ye, X., Wang, J., Hsieh, M.-J., Cui, G., Roe, D.R., Mathews, D.H., Seetin, M.G., Sagui, C., Babin, V., Luchko, T., Gusarov, S., Kovalenko, A., Kollman P. A.: AMBER 11; University of California, San Francisco, 2010.

(47) Deng, L., Broom, A., Kitova, E.N., Richards, M.R., Zheng, R.B., Shoemaker, G.K., Meiering, E.M., Klassen, J.S.: Kinetic stability of the streptavidin-biotin interaction enhanced in the gas phase. *J. Am. Chem. Soc*. **134**, 16586-16596 (2012)

(48) Vanquelef, E., Simon, S., Marquant, G., Garcia, E., Klimerak, G., Delepine, J. C., Cieplak, P., Dupradeau, F.-Y.: Server: a web service for deriving RESP and ESP charges

and building force field libraries for new molecules and molecular fragments. *Nucleic Acids Res.* **39**, W511−W517 (2011)

(49) Dupradeau, F.-Y., Pigache, A., Zaffran, T., Savineau, C., Lelong, R., Grivel, N., Lelong, D., Rosanski, W., Cieplak, P.: The R.E.D. tools: advances in RESP and ESP charge derivation and force field library building. *Phys. Chem. Chem. Phys.* **12**, 7821−7839 (2010)

(50) Frisch, M.J., Trucks, G.W., Schlegel, H.B., Scuseria, G.E., Robb, M.A., Cheeseman, J.R., Scalmani, G., Barone, V., Mennucci, B., Petersson, G.A., Nakatsuji, H., Caricato, M., Li, X., Hratchian, H.P., Izmaylov, A.F., Bloino, J., Zheng, G., Sonnenberg, J.L., Hada, M., Ehara, M., Toyota, K., Fukuda, R., Hasegawa, J., Ishida, M., Nakajima, T., Honda, Y., Kitao, O., Nakai, H., Vreven, T., Montgomery, J.A., Jr., Peralta, J.E., Ogliaro, F., Bearpark, M., Heyd, J.J., Brothers, E., Kudin, K.N., Staroverov, V.N., Kobayashi, R., Normand, J., Raghavachari, K., Rendell, A., Burant, J.C., Iyengar, S.S., Tomasi, J., Cossi, M., Rega, N., Millam, J.M., Klene, M., Knox, J.E., Cross, J.B., Bakken, V., Adamo, C., Jaramillo, J., Gomperts, R., Stratmann, R.E., Yazyev, O., Austin, A.J., Cammi, R., Pomelli, C., Ochterski, J. W., Martin, R. L., Morokuma, K., Zakrzewski, V.G., Voth, G.A., Salvador, P., Dannenberg, J.J., Dapprich, S., Daniels, A.D., Farkas, Ö., Foresman, J.B., Ortiz, J.V., Cioslowski, J., Fox, D.J.: Gaussian 09, Revision A.1; Gaussian, Inc.: Wallingford, CT, 2009.

(51) Merritt, E.A., Kuhn, P., Sarfaty, S., Erbe, J.L., Holmes, R.K., Hol, W.G.: The 1.25 A resolution refinement of the cholera toxin B-pentamer: evidence of peptide backbone strain at the receptor-binding site. *J. Mol. Biol.* **282**, 1043-1059 (1998)

(52) Boyle, N.M.O'., Banck, M., James, C.A., Morley, C., Vandermeersch, T., Hutchison, G.R.: Open Babel: An open chemical toolbox. *J. Cheminf*. **3**, 33. DOI:10.1186/1758-2946-3-33 (2011)

(53) The Open Babel Package, version 2.3.1 http://openbabel.org

(54) Hall, Z., Politis, A., Bush, M.F., Smith, L.J., Robinson, C.V.: Charge-state dependent compaction and dissociation of protein complexes: insights from ion mobility and molecular dynamics. *J. Am. Chem. Soc*. **134**, 3429-3438 (2012)

(55) Wang, J., Wang, W., Kollman, P.A., Case, D.A.: Automatic atom type and bond type perception in molecular mechanical calculations. *J. Mol. Graphics Modell*. **25**, 247−260 (2006)

(56) Duan, Y., Wu, C., Chowdhury, S., Lee, M.C., Xiong, G., Zhang, W., Yang, R., Cieplak, P., Luo, R., Lee, T., Caldwell, J., Wang, J., Kollman, P. J.: A point-charge force field for molecular mechanics simulations of proteins based on condensed-phase quantum mechanical calculations. *Comput. Chem*. **24**, 1999−2012 (2003)

(57) Wang, J., Wolf, R.M., Caldwell, J.W., Kollman, P.A., Case, D.A.: Development and testing of a general Amber force field. *J. Comput. Chem*. **25**, 1157−1174 (2004)

(58) Phillips, J.C., Braun, R., Wang, W., Gumbart, J., Tajkhorshid, E., Villa, E., Chipot, C., Skeel, R.D., Kalé, L., Schulten, K.: Scalable molecular dynamics with NAMD, *J. Comput. Chem.* **26**, 1781−1802 (2005)

(59) Sun, J., Kitova, E.N., Wang, W., Klassen, J.S.: Method for distinguishing specific and nonspecific protein-ligand complexes in nanoelectrospray ionization mass spectrometry. *Anal. Chem*. **78**, 3010-3018 (2006)

(60) Wang, W., Kitova, E.N., Klassen, J.S.: Nonspecific protein-carbohydrate complexes produced by nanoelectrospray ionization. Factors influencing their formation and stability. *Anal. Chem.* **77**, 3060-3071 (2005)

(61) Holmgren, J., Lönnroth, I., Månsson, J., Svennerholm, L.: Interaction of cholera toxin and membrane GM1 ganglioside of small intestine. *Proc. Natl. Acad. Sci.* **72**, 2520-2524 (1975)

(62) Kitova, E.N., Bundle, D.R., Klassen, J.S.: Thermal dissociation of protein-oligosaccharide complexes in the gas phase. Mapping the intrinsic intermolecular interactions. *J. Am. Chem. Soc.* **124**, 5902-5913 (2002)

(63) Kitova, E.N., Seo, M., Roy, P.-N., Klassen, J.S.: Elucidating the intermolecular interactions within a desolvated protein-ligand complex. An experimental and computational study. *J. Am. Chem. Soc.* **130**, 1214-1226 (2008)

(64) Liu, L., Bagal, D., Kitova, E.N., Schnier, P.D., Klassen, J.S.: Hydrophobic protein-ligand interactions preserved in the gas phase. *J. Am. Chem. Soc.* **131**, 15980–15981 (2009)

(65) E.N. Kitova, D.R. Bundle and J.S. Klassen "Partitioning of Solvent Effects and Intrinsic Interactions in Biological Recognition" Angew. Chemie Int. Ed. 2004, 43, 4183-4186.

(66) E.N. Kitova, D.R. Bundle and J.S. Klassen "Evidence for the Preservation of Specific Intermolecular Interactions in Gaseous Protein-Oligosaccharide Complexes" J. Am. Chem. Soc. 2002, 124, 9340-9341.

(67) Liu, L., Michelsen, K., Kitova, E.N., Schnier, P.D., Klassen, J.S.: Energetics of lipid binding in a hydrophobic protein cavity. J. Am. Chem. Soc. 134, 3054-3060 (2012)

(68) Light-Wahl, K.J., Schwartz, B.L., Smith, R.D.: Observation of the noncovalent quaternary associations of proteins be electrospray ionization mass spectrometry. *J. Am. Chem. Soc*. **116**, 5271–5278 (1994)

(69) Jurchen, J.C., Garcia, D.E., Williams, E.R.: Further studies on the origins of asymmetric charge partitioning in protein homodimers. *J. Am. Soc. Mass Spectrom.* **15**, 1408–1415 (2004)

(70) Pagel, K., Hyung, S.J., Ruotolo, B.T., Robinson, C.V.: Alternate dissociation pathways identified in charge-reduced protein complex ions. *Anal. Chem.* **82**, 5363-5372 (2010)

(71) Liu, L., Michelsen, K., Kitova, E.N., Schnier, P.D., Klassen, J.S.: Evidence that water can reduce the kinetic stability of protein−hydrophobic ligand interactions. *J. Am. Chem. Soc.* **132**, 17658–17660 (2010)

(72) Salpin, J-Y., Tortajada, J.: Gas-phase acidity of D-glucose. A density functional theory study. *J. Mass Spectrom*. **39**, 930-941 (2004)

(73) Sinelnikov, I., Kitova, E.N., Klassen, J.S.: Influence of coulombic repulsion on dissociation pathways and energetics of multiprotein complexes in the gas phase. *J. Am. Soc. Mass Spectrom.* **18**, 617-631 (2007)

Table 1. Average charge states (*ACS*) of the CTB, (CTB + GM1) and (CTB + GM1-Cer) product ions observed by CID of protonated and deprotonated $(CTB_5 + 5GM1)^{n+/-}$, $(CTB_5 + 5GM1\text{-}Cer)^{n+/-}$ and $(CTB_5)^{n+/-}$ ions.

Parent ion	n (charge state of parent ion)	x (*ACS* of leaving CTB)	y (*ACS* of leaving (CTB+GM1))	(x/n)%	(y/n)%
$(CTB_5 + 5GM1)$	14+	$(5.3 \pm 0.1)+$	$(4.8 \pm 0.1)+$	38%	34%
	15+	$(5.9 \pm 0.1)+$	$(5.6 \pm 0.1)+$	39%	37%
	12-	$(4.8 \pm 0.1)-$	n/a	40%	n/a
	13-	$(4.9 \pm 0.1)-$	$(5.3 \pm 0.3)-$ [a]	38%	41%
	14-	$(5.2 \pm 0.1)-$	$(5.5 \pm 0.1)-$ [a]	37%	39%
$(CTB_5 + 5GM1\text{-}Cer)$	14+	$(5.2 \pm 0.1)+$	5+ [b]	37%	36%
	15+	$(5.9 \pm 0.1)+$	$(5.7 \pm 0.1)+$	39%	38%
	16+	$(6.5 \pm 0.1)+$	$(6.4 \pm 0.1)+$	41%	40%
	13-	$(4.8 \pm 0.1)-$	n/a	37%	n/a
	14-	$(5.0 \pm 0.1)-$	6- [a,b]	36%	43%
	15-	$(5.4 \pm 0.2)-$	$(5.3 \pm 0.4)-$ [a]	36%	35%
CTB_5 [c]	14+	$(5.3 \pm 0.1)+$	n/a	38%	n/a
	15+	$(5.9 \pm 0.1)+$	n/a	39%	n/a
	16+	$(6.3 \pm 0.1)+$	n/a	39%	n/a
	12-	$(5.0 \pm 0.1)-$	n/a	42%	n/a
	13-	$(5.1 \pm 0.1)-$	n/a	39%	n/a
	14-	$(5.5 \pm 0.1)-$	n/a	39%	n/a

a. These product ions were observed only at higher collision energies (>40V).

b. Only a single charge state was observed.

c. CID mass spectra not shown.

a. $(CTB_5 + 5GM1)^{n+}$ $\longrightarrow$ $(CTB_4 + 5GM1)^{(n-x)+} + CTB^{x+}$

$\longrightarrow$ $(CTB_4 + 4GM1)^{(n-y)+} + (CTB + GM1)^{y+}$

$(CTB_5 + 5GM1\text{-}Cer)^{n+}$ $\longrightarrow$ $(CTB_4 + 5GM1\text{-}Cer)^{(n-x)+} + CTB^{x+}$

$\longrightarrow$ $(CTB_4 + 4GM1\text{-}Cer)^{(n-y)+} + (CTB + GM1\text{-}Cer)^{y+}$

b. $(CTB_5 + 5GM1)^{n-}$ $\longrightarrow$ $(CTB_5 + 4GM1)^{(n-1)-} + GM1^-$

$\longrightarrow$ $(CTB_4 + 4GM1)^{(n-y)-} + (CTB + GM1)^{y-}$

$\longrightarrow$ $(CTB_4 + 5GM1)^{(n-x)-} + CTB^{x-}$

$(CTB_5 + 5GM1\text{-}Cer)^{n-}$ $\longrightarrow$ $(CTB_5 + 4GM1\text{-}Cer)^{(n-1)-} + GM1\text{-}Cer^-$

$\longrightarrow$ $(CTB_4 + 4GM1\text{-}Cer)^{(n-y)-} + (CTB + GM1\text{-}Cer)^{y-}$

$\longrightarrow$ $(CTB_4 + 5GM1\text{-}Cer)^{(n-x)-} + CTB^{x-}$

c. $(S_4 + 4B)^{n+}$ $\longrightarrow$ $(S_4 + 3B)^{n+} + B$

$\longrightarrow$ $(S_4 + 3B)^{(n-1)+} + B^+$

$\longrightarrow$ $(S_3 + 4B)^{(n-x)+} + S^{x+}$

$(S_4 + 4Btl)^{n+}$ $\longrightarrow$ $(S_3 + 4Btl)^{(n-x)+} + S^{x+}$

$\longrightarrow$ $(S_3 + 3Btl)^{(n-y)+} + (S + Btl)^{y+}$

d. $(S_4 + 4B)^{n-}$ $\longrightarrow$ $(S_4 + 3B)^{n-} + B$

$\longrightarrow$ $(S_4 + 3B)^{(n-1)-} + B^-$

$(S_4 + 4Btl)^{n-}$ $\longrightarrow$ $(S_4 + 3Btl)^{(n-1)-} + Btl^-$

Scheme 1. Summary of CID pathways observed for (a) $(CTB_5 + 5GM1)^{n+}$, n = 14 and 15, and $(CTB_5 + 5GM1\text{-}Cer)^{n+}$, n = 14 − 16; (b) $(CTB_5 + 5GM1)^{n-}$, n = 12 − 14, and $(CTB_5 + 5GM1\text{-}Cer)^{n-}$, n = 13 − 15; (c) $(S_4 + 4B)^{n+}$ and $(S_4 + Btl)^{n+}$, n = 15 and 16; and (d) $(S_4+4B)^{n-}$, n = 12 and 13, and $(S_4+4Btl)^{n-}$, n = 11 − 13.

Figure captions

Figure 1. NanoESI mass spectra acquired in (a) positive and (b) negative ion mode for an aqueous ammonium acetate (200 mM) solution of (6 μM) CTB$_5$ subunit and (38 μM) GM1 ($\equiv$ L).

Figure 2. CID mass spectra of the $(CTB_5 + 5L)^{14+}$ ion, where L $\equiv$ GM1, at a collision energy of (a) 30 V, (b) 40 V, (c) 50 V and (d) 60 V.

Figure 3. CID mass spectra of the $(CTB_5 + 5L)^{14-}$ ion, where L $\equiv$ GM1, at a collision energy of (a) 10 V, (b) 30 V and (c) 50 V.

Figure 4. CID mass spectra of the $(CTB_5 + 5L)^{14+}$ ion, where L $\equiv$ GM1-Cer, at a collision energy of (a) 30 V, (b) 40 V, (c) 50 V, and (d) 60 V.

Figure 5. CID mass spectra of the $(CTB_5 + 5L)^{14-}$ ion, where L $\equiv$ GM1-Cer, at a collision energy of (a) 10 V, (b) 30 V and (c) 55 V.

Supplementary Information for:
   Dissociation of Multisubunit Protein-Ligand Complexes in the Gas Phase.

Evidence for Ligand Migration

Yixuan Zhang, Lu Deng, Elena N. Kitova, and John S. Klassen

Table S1. Charge configurations considered for the MD simulations performed on the $(CTB_5 + 5GM1)^{15+}$ and $(CTB_5 + 5GM1)^{14-}$ ions.

Configuration	Subunit	Protonated residues
B15_1	D	NThr 01, Lys 23,34, 62, 91, His 13, 18
	E, F, G and H	His 13, Lys 43
B15_2	D	NThr 01, Lys 23, 34, 63, 91, His 13, 18
	E, F, G and H	His 13, Lys 43
B15_3	D	NThr 01, Lys 43,34, 62, 91, His 13, 18
	E, F, G and H	His 13, Lys 43
B15_4	D	NThr 01, Lys 43, 34, 63, 91, His 13, 18
	E, F, G and H	His 13, Lys 43
B15_5	D	NThr 01, Lys 81,34, 62, 91, His 13, 18
	E, F, G and H	His 13, Lys 43
B15_6	D	NThr 01, Lys 81, 34, 63, 91, His 13, 18
	E, F, G and H	His 13, Lys 43
B15_7	D	NThr 01, Lys 43, 34, 63, Arg 94, His 13, 18
	E, F, G and H	His 13, Lys 43
B15_8	D	NThr 01, Lys 43, 34, 62, Arg 94, His 13, 18
	E, F, G and H	His 13, Lys 43
B15_9	D	NThr 01, Lys 23, 34, 63, Arg 94, His 13, 18
	E, F, G and H	His 13, Lys 43
B15_10	D	NThr 01, Lys 23, 34, 62, Arg 94, His 13, 18
	E, F, G and H	His 13, Lys 43
B15_11	D	NThr 01, Lys 81, 34, 63, Arg 94, His 13, 18
	E, F, G and H	His 13, Lys 43
B15_12	D	NThr 01, Lys 81, 34, 62, Arg 94, His 13, 18
	E, F, G and H	His 13, Lys 43
		Deprotonated residues
B9_1	D	Glu 11, 51, 79, 83, Asp 59
	E, F, G and H	Asp 22

Table S2. Average charge states (*ACS*) of the lS subunit and (S + Btl) product ions observed by CID of protonated and deprotonated $(S_4 + 4B)^{n+/-}$ and $(S_4 + 4Btl)^{n+/-}$ ions.

Parent ion	n (charge state of parent ion)	x (*ACS* of leaving S)	y (*ACS* of leaving (S+Btl))	(x/n)%	(y/n)%
$(S_4 + 4B)$	15+	$(6.8 \pm 0.1)+$	n/a	45%	n/a
	16+	$(6.9 \pm 0.1)+$	n/a	43%	n/a
	12-	n/a	n/a	n/a	n/a
	13-	n/a	n/a	n/a	n/a
$(S_4 + 4Btl)$	15+	$(7.1 \pm 0.1)+$	$(6.8 \pm 0.1)+$	47%	45%
	16+	$(7.3 \pm 0.1)+$	$(6.9 \pm 0.1)+$	46%	43%
	11-	n/a	n/a	n/a	n/a
	12-	n/a	n/a	n/a	n/a
	13-	n/a	n/a	n/a	n/a

GM1
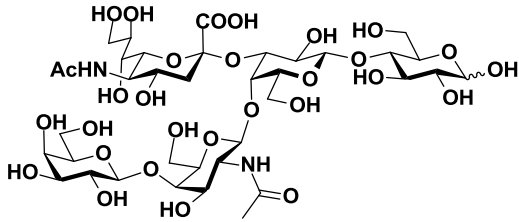
GM1-Cer, *d*18:1-18:0
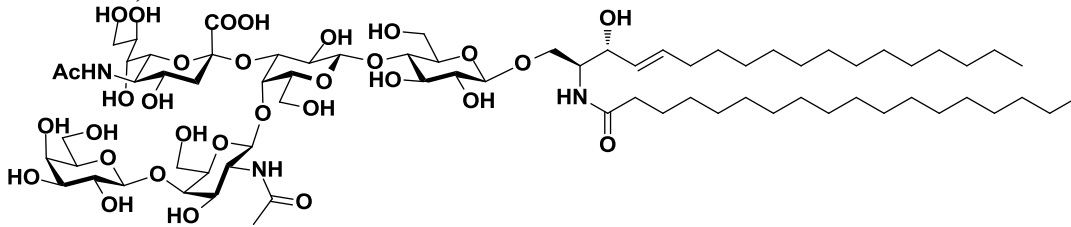
GM1-Cer, *d*20:1-18:0
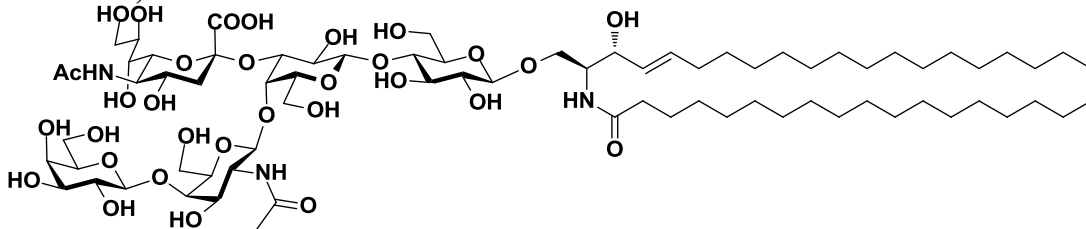
Biotin
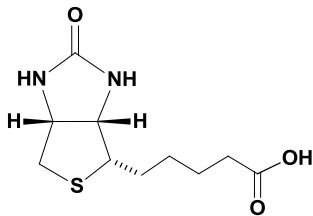
1,2-dipalmitoyl-*sn*-glycero-3-phosphoethanolamine-N-(biotinyl)
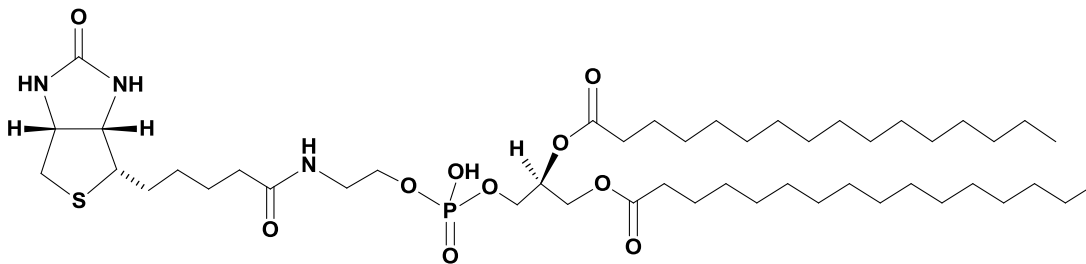
Figure S1. Structures of GM1, GM1-Cer (*d*18:1-18:0 and *d*20:1-18:0), biotin (B) and

1,2-dipalmitoyl-*sn*-glycero-3-phosphoethanolamine-N-(biotinyl) (Btl).
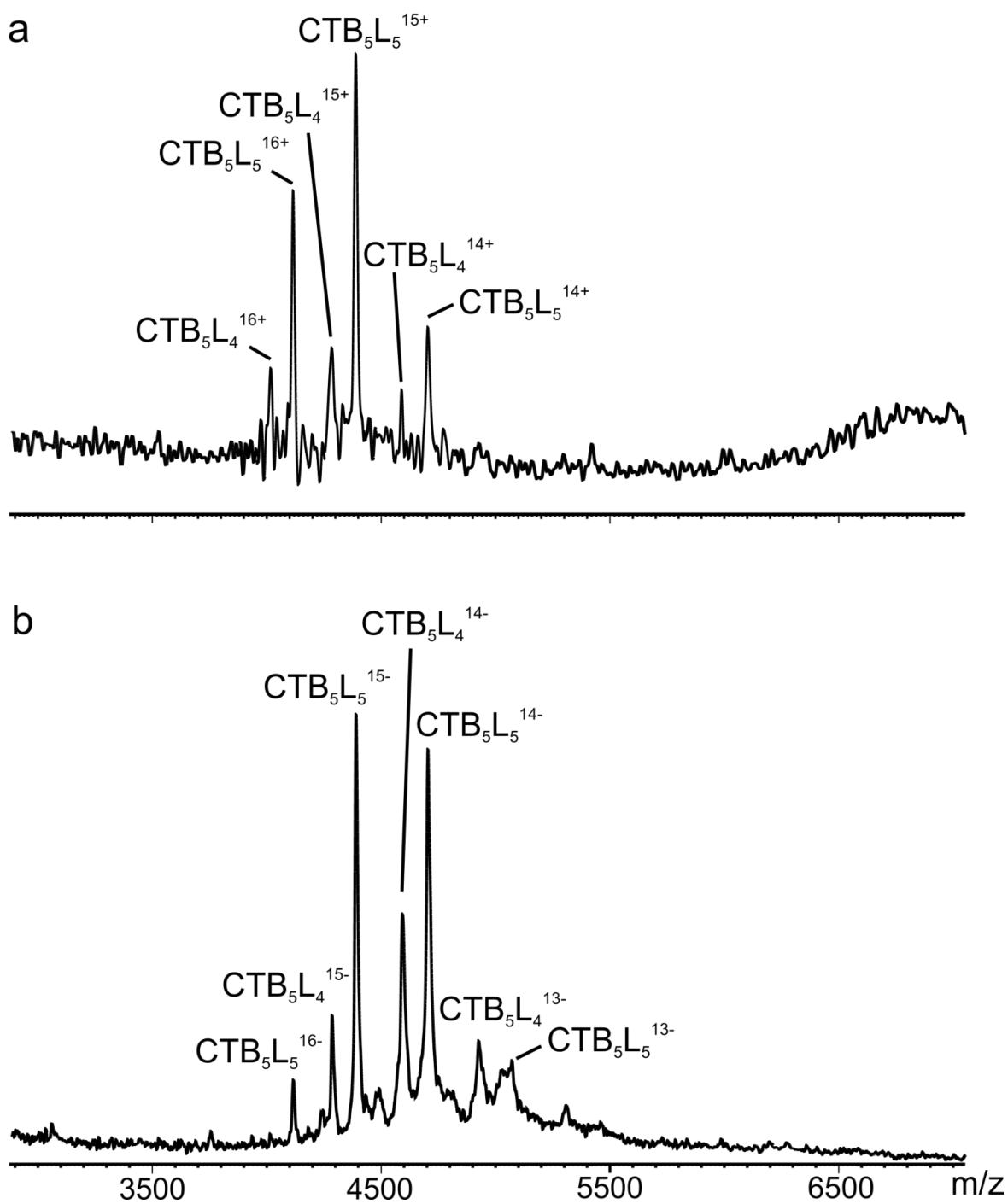
Figure S2. ESI mass spectra acquired in (a) positive and (b) negative ion mode for aqueous ammonium acetate (200 mM) solution of (6 μM) CTB$_5$ subunit and (10 μM) ND containing 8% GM1-Cer ($\equiv$ L).
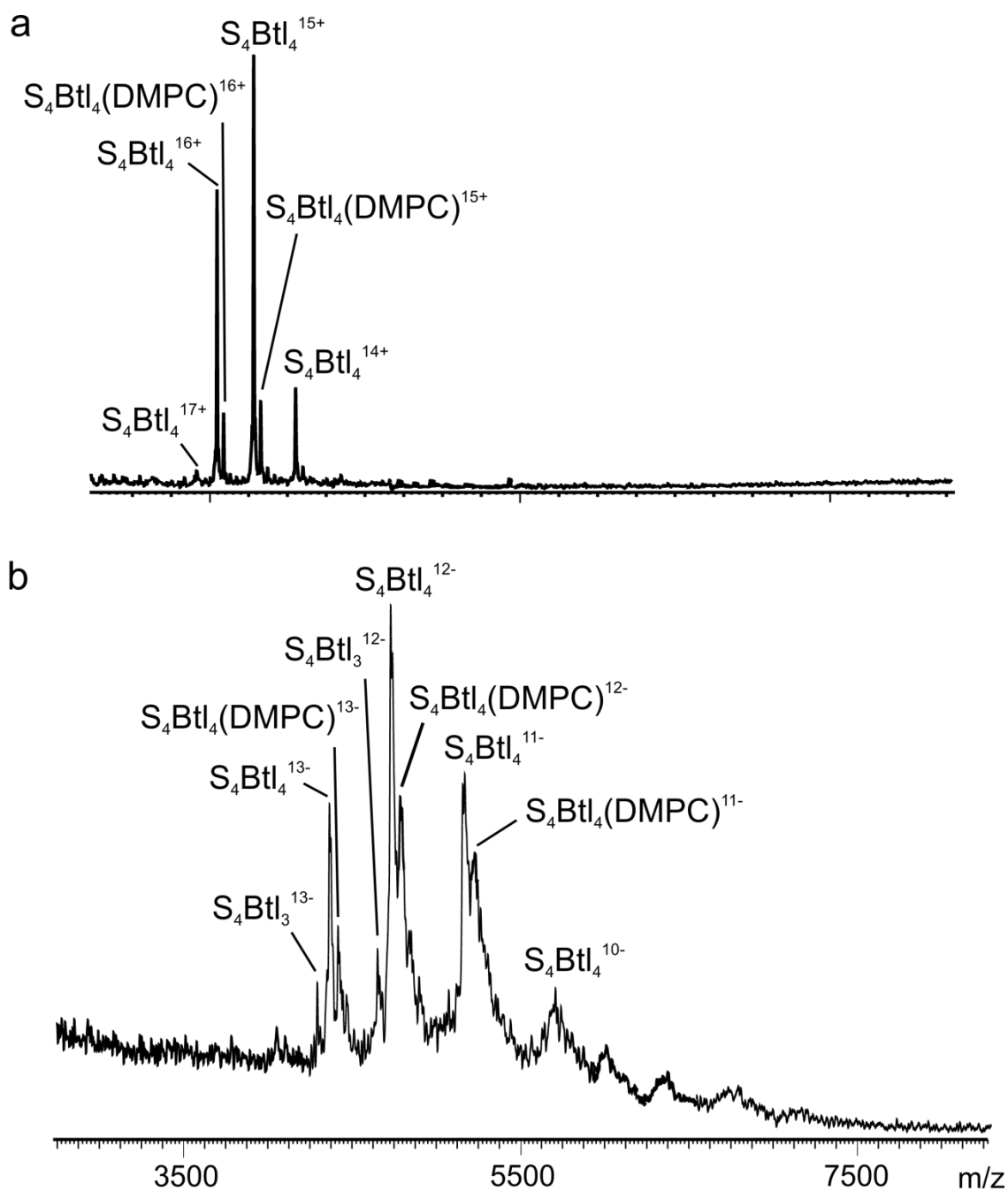
Figure S3. ESI mass spectra acquired in (a) positive and (b) negative ion mode for aqueous ammonium acetate (200 mM) solution of (5 μM) streptavidin and (10 μM) ND containing 8% Btl. Nonspecific binding between DMPC and Btl is likely responsible for the appearance of the $S_4Btl_4(DMPC)^{n+/-}$ ions.

41
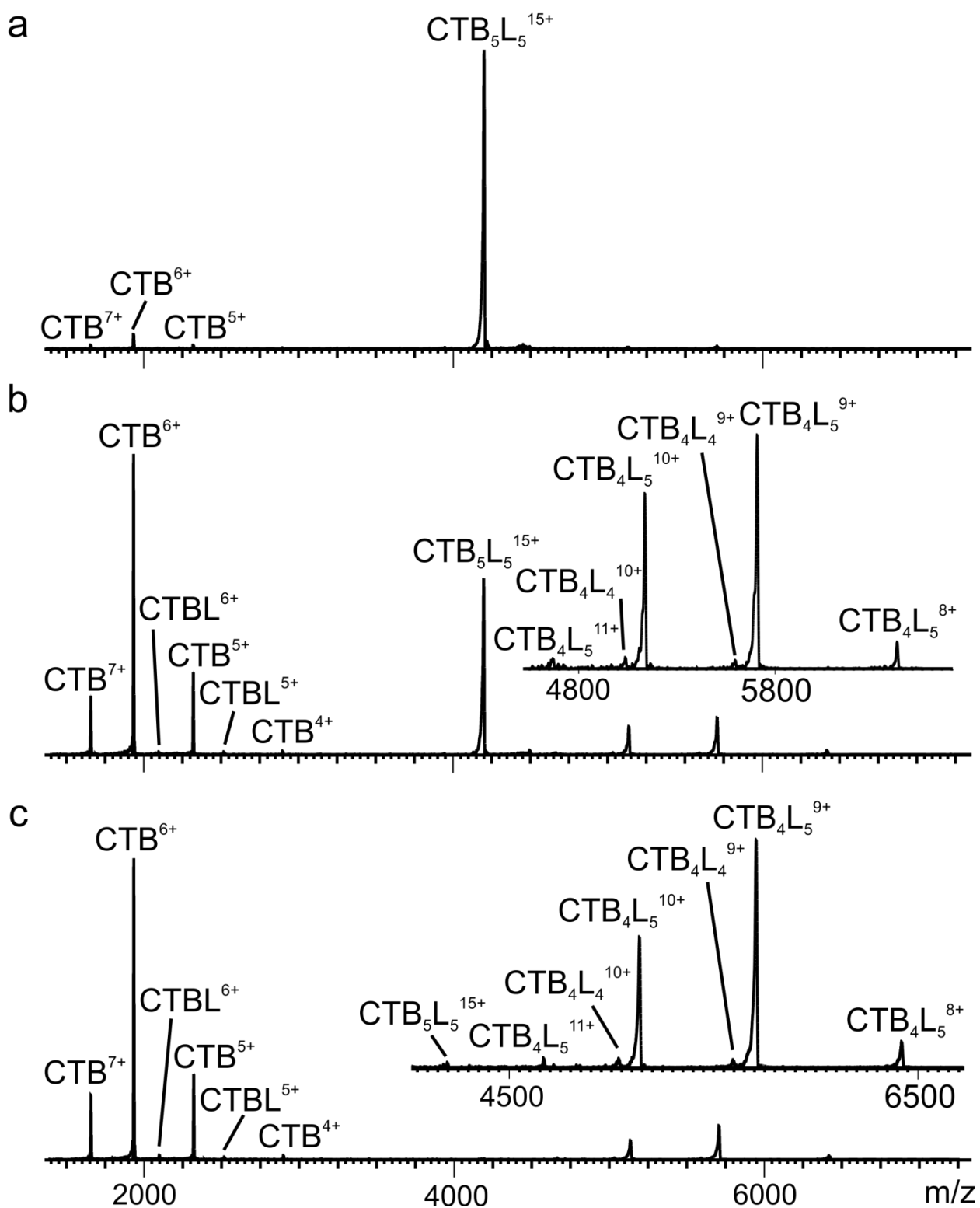
Figure S4. CID mass spectra in positive mode of the $(CTB_5 + 5L)^{15+}$ ion (where L = GM1) at a collision energy of (a) 20 V, (b) 40 V and (c) 50 V.

a

$CTB_5L_5^{13-}$

$CTB_5L_4^{12-}$

L^-

b

L^-

$CTB_5L_4^{12-}$

$CTB_5L_5^{13-}$ $CTB_5L_3^{11-}$

CTB^{5-}

$CTB_5L_2^{10-}$

c

CTB^{6-}

x5

L^-

$CTBL^{6-}$

1900   2100

$CTB_4L_5^{9-}$

$CTB_5L_2^{10-}$

$CTB_5L_3^{11-}$

$CTB_4L_4^{8-}$

$CTB_5L_4^{12-}$

$CTB_4L_5^{8-}$ CTB_5L^{9-}

CTB^{5-}

$CTB_5L_5^{13-}$

CTB^{6-} CTB^{4-}

$CTB_4L_4^{7-}$

2000   4000   6000   8000   m/z
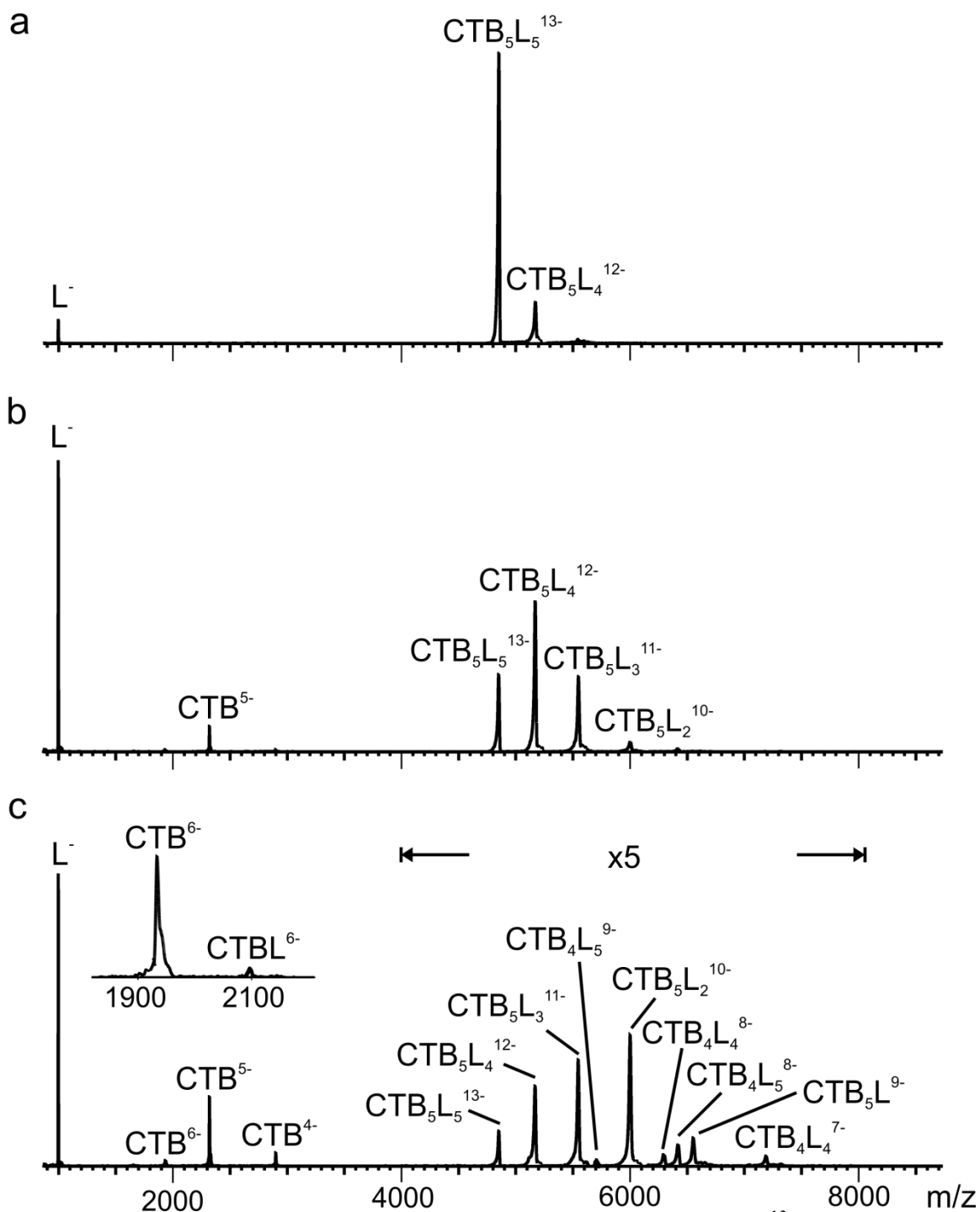
Figure S5. CID mass spectra in negative mode of the $(CTB_5 + 5L)^{13-}$ ion (where L =
GM1), at a collision energy of (a) 10 V, (b) 30 V and (c) 50 V. The intensities
in the m/z range 4000 – 8000 (c) were magnified x5.
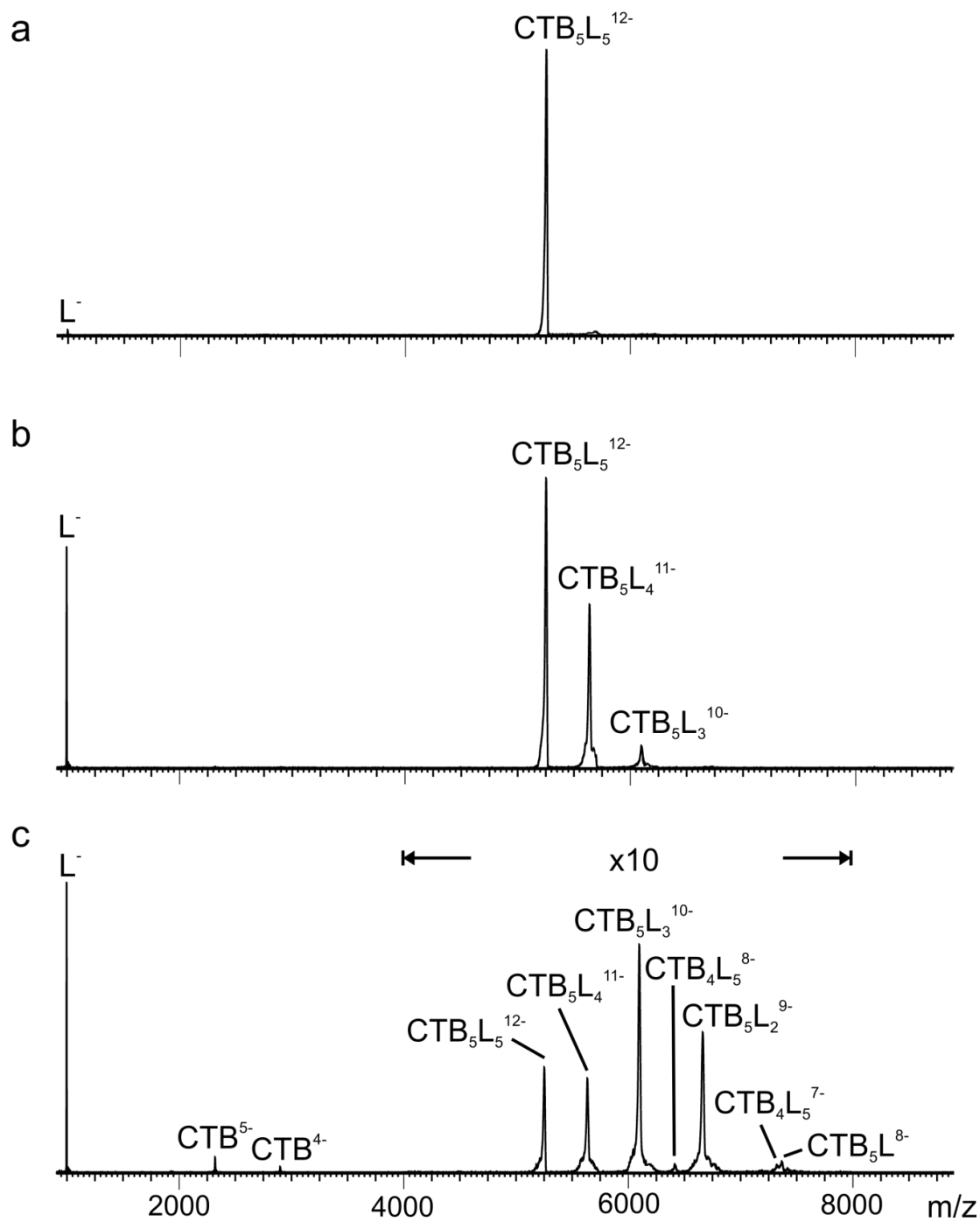
Figure S6. CID mass spectra in negative mode of the $(CTB_5 + 5L)^{12-}$ ion (where L = GM1) at a collision energy of (a) 10 V, (b) 30 V and (c) 60 V. The intensities in the m/z range 4000 – 8000 (c) were magnified x10.
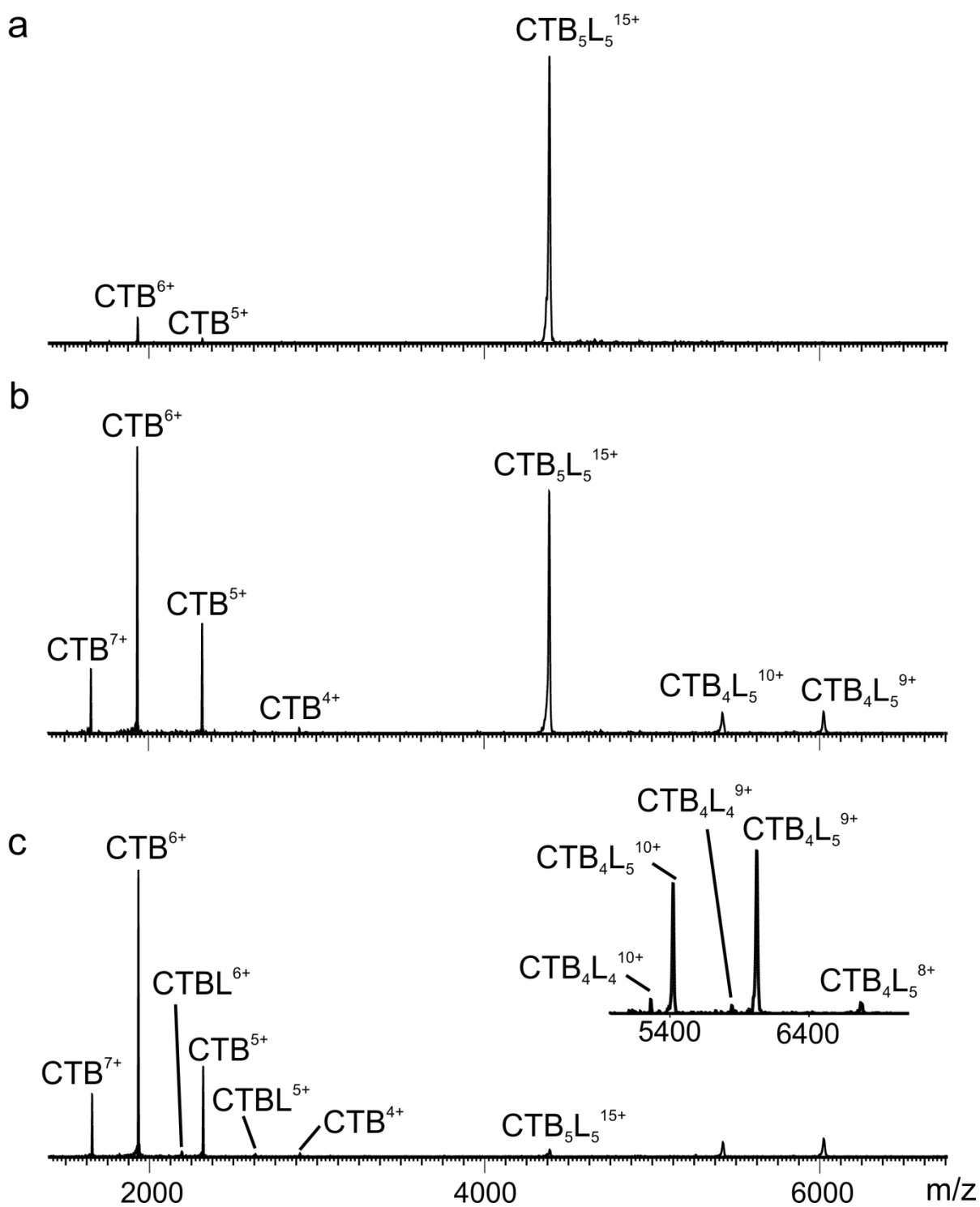
Figure S7. CID mass spectra in positive mode of the $(CTB_5 + 5L)^{15+}$ ion (where L = GM1-Cer) at a collision energy of (a) 20 V, (b) 40 V and (c) 50 V.
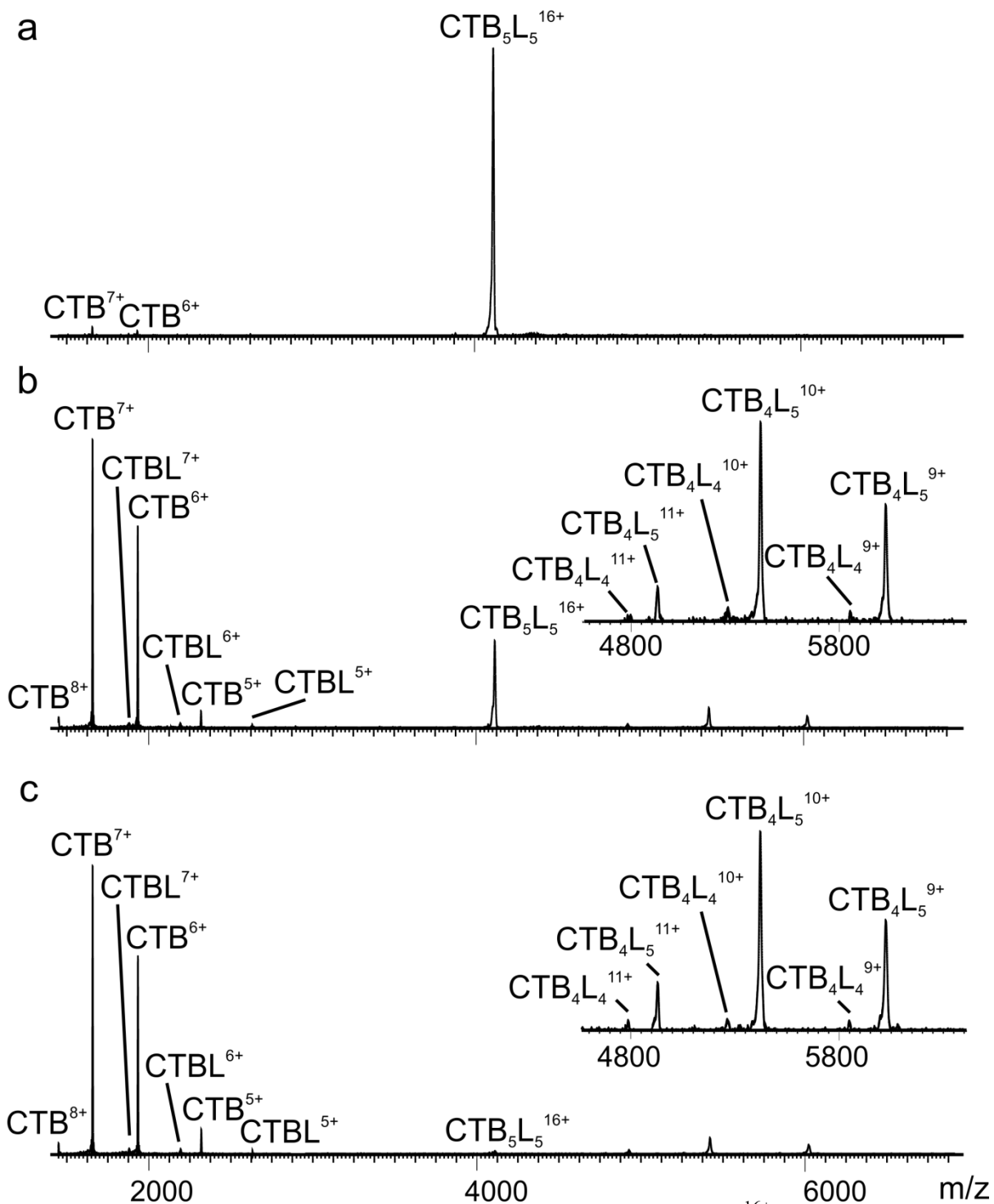
Figure S8. CID mass spectra in positive mode of the $(CTB_5 + 5L)^{16+}$ ion (where L = GM1-Cer) at a collision energy of (a) 20 V, (b) 40 V and (c) 50 V.
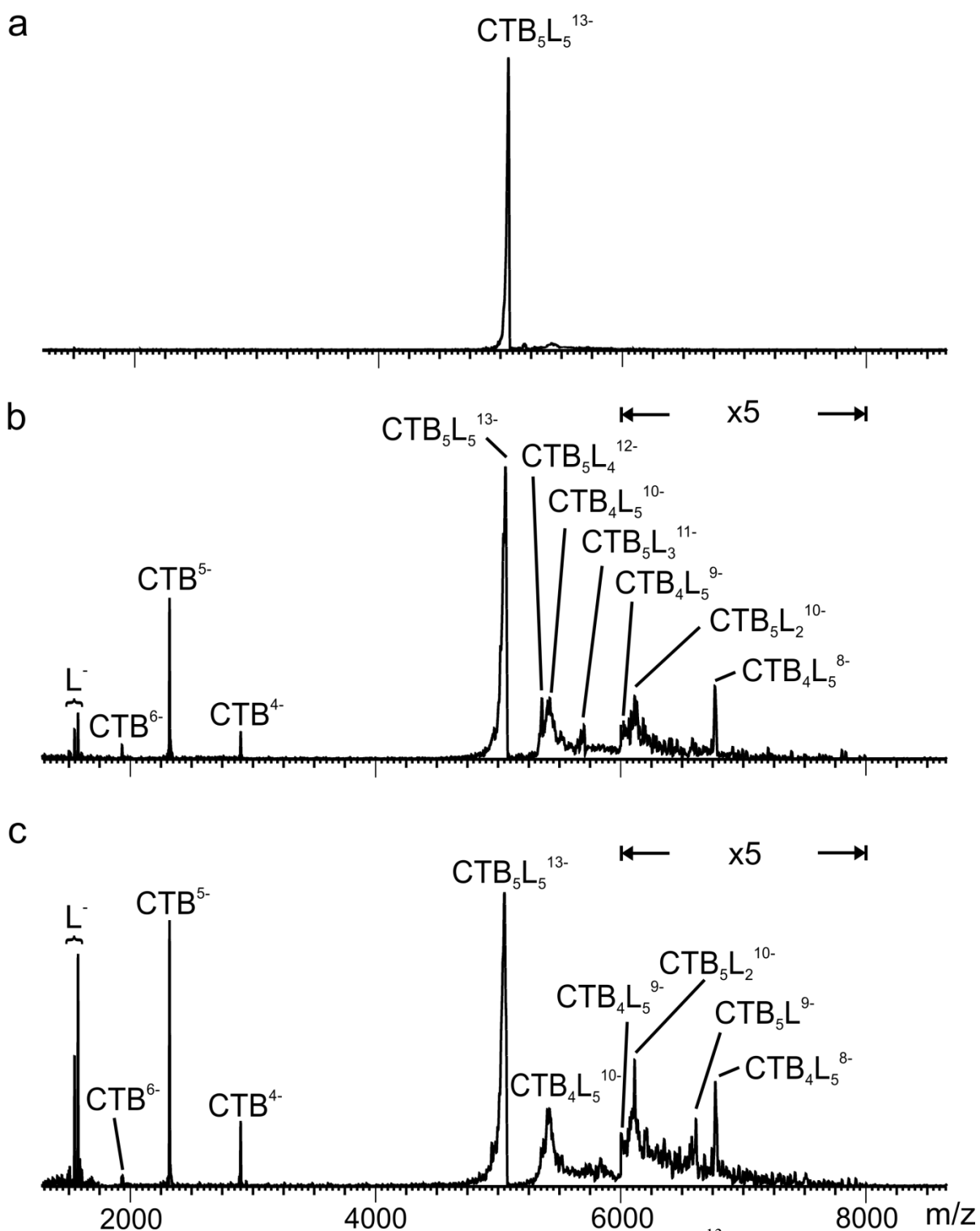
Figure S9. CID mass spectra in negative mode of the $(CTB_5 + 5L)^{13-}$ ion, ion (where L = GM1-Cer) at a collision energy of (a) 10 V, (b) 45 V and (c) 65 V. In (b) and (c) the intensities in the m/z range 6000 - 8000 were magnified x5.

47

a

$CTB_5L_5^{15-}$

$CTB_5L_4^{14-}$

b

x5

$CTB_5L_5^{15-}$

$CTB_5L_4^{14-}$

$CTB_5L_3^{13-}$

L^-

CTB^{7-}

CTB^{6-} CTB^{5-}

$CTB_4L_4^{9-}$

$CTB_5L_2^{12-}$ $CTB_4L_5^{9-}$

c

x5

CTB^{4-}

CTB^{5-}

$CTB_4L_2^{9-}$

$CTB_4L_5^{10-}$ $CTB_4L_3^{9-}$

CTB^{7-}

$CTB_5L_2^{12-}$ $CTB_4L_4^{9-}$ $CTB_4L_5^{9-}$

L^- CTB^{6-} $CTBL^{5-}$

$CTB_5L_3^{13-}$

2600   2900

$CTB_5L_4^{14-}$ $CTB_4L_2^{8-}$

$CTB_5L_5^{15-}$ $CTB_4L_3^{8-}$

CTB^{4-} $CTB_4L_4^{8-}$

$CTB_4L_5^{8-}$

2000   4000   6000   m/z
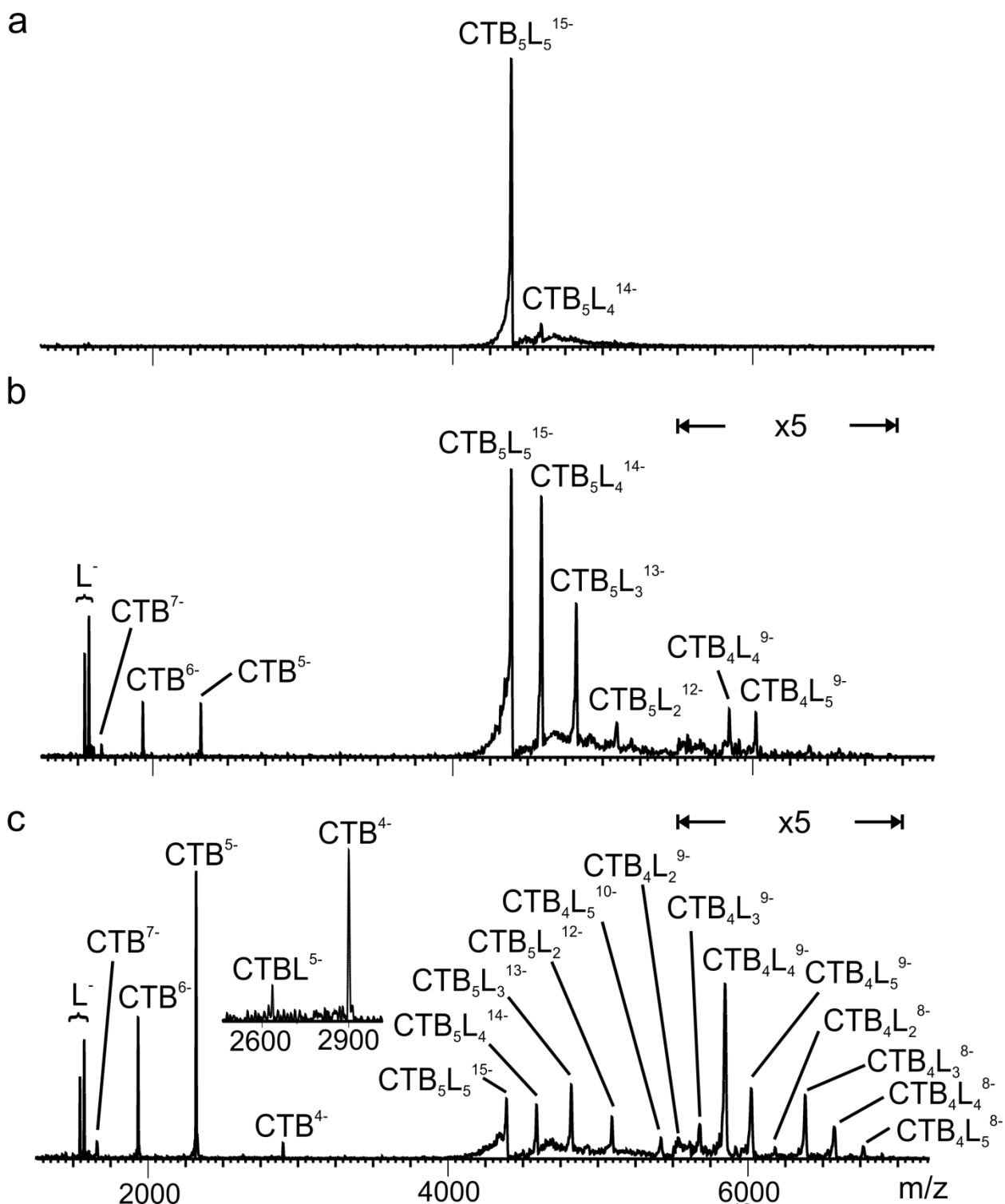
Figure S10. CID mass spectra in negative mode of the $(CTB_5 + 5L)^{15-}$ ion (where L =

GM1-Cer) at a collision energy of (a) 10 V, (b) 30 V and (c) 40 V. In (b)

and (c) the intensities in the m/z range 5500 - 7000 were magnified x5.
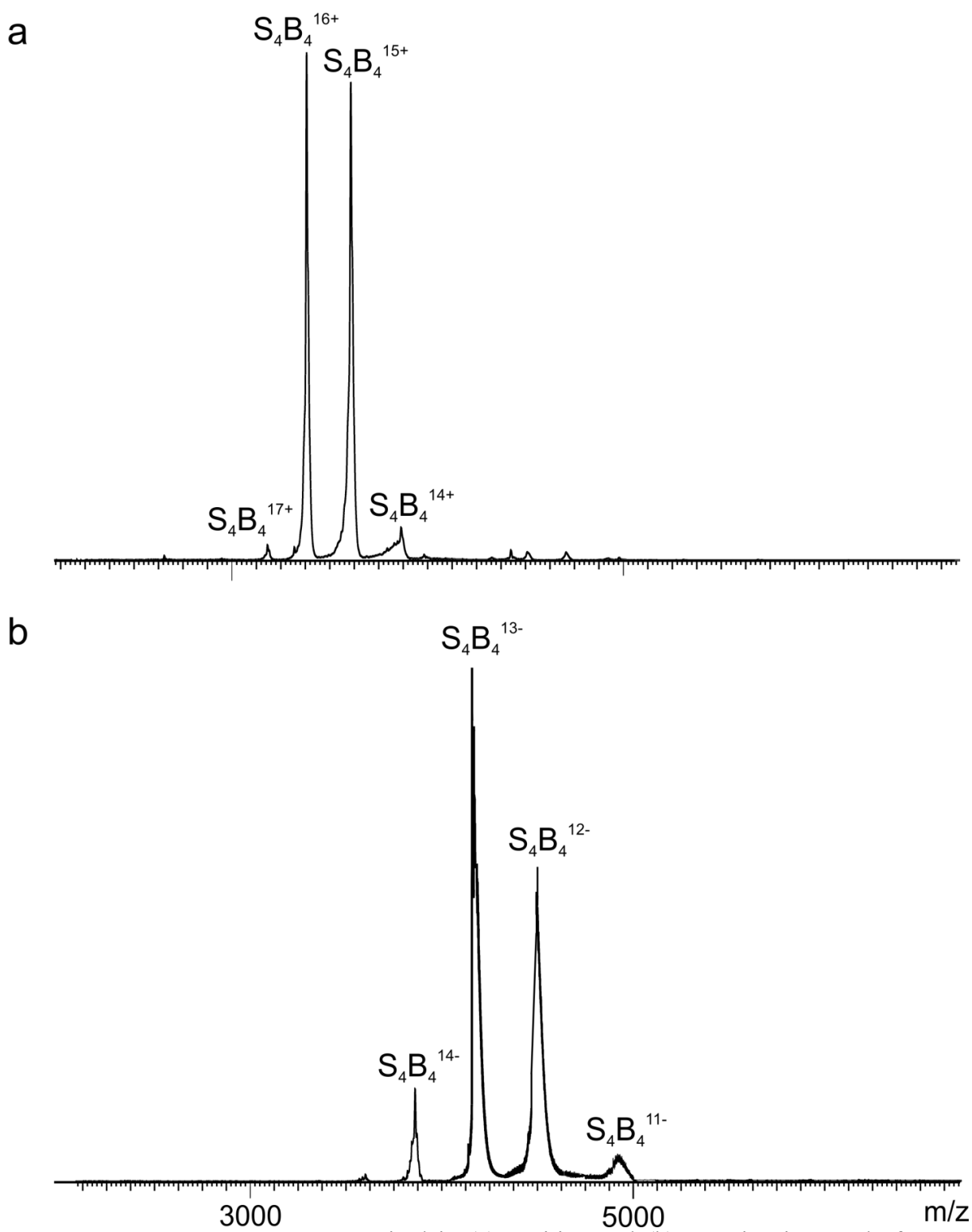
Figure S11. ESI mass spectra acquired in (a) positive and (b) negative ion mode for aqueous ammonium acetate (200 mM) solution of (5 μM) S_4 and (20 μM) B.
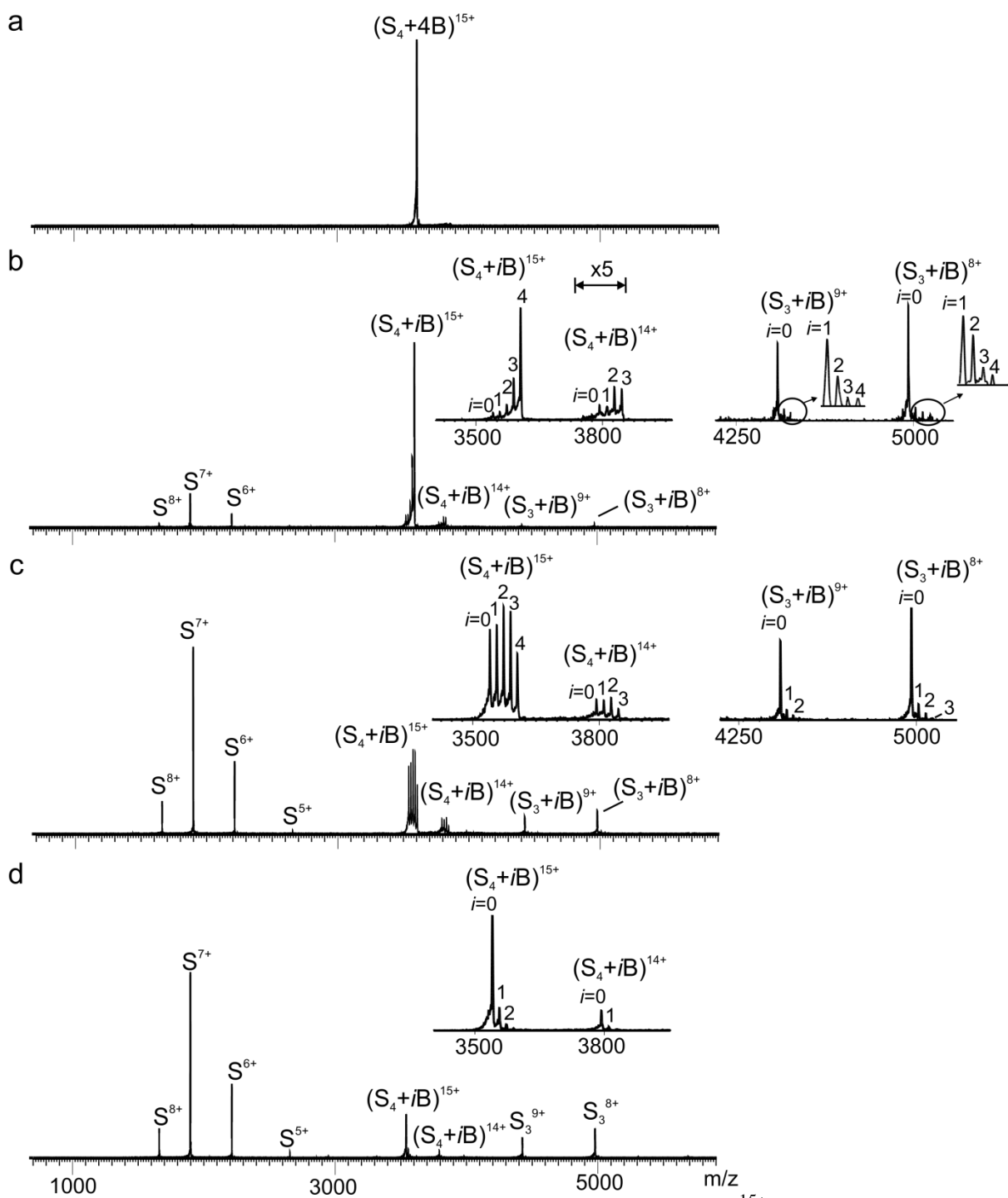
**Figure S12**. CID mass spectra in positive mode of the $(S_4 + 4B)^{15+}$ ion at a collision energy of (a) 3 V, (b) 26 V, (c) 32 V, and (d) 38 V. In the inset of (b), the intensities in the m/z range 3750 - 3850 were magnified x5.
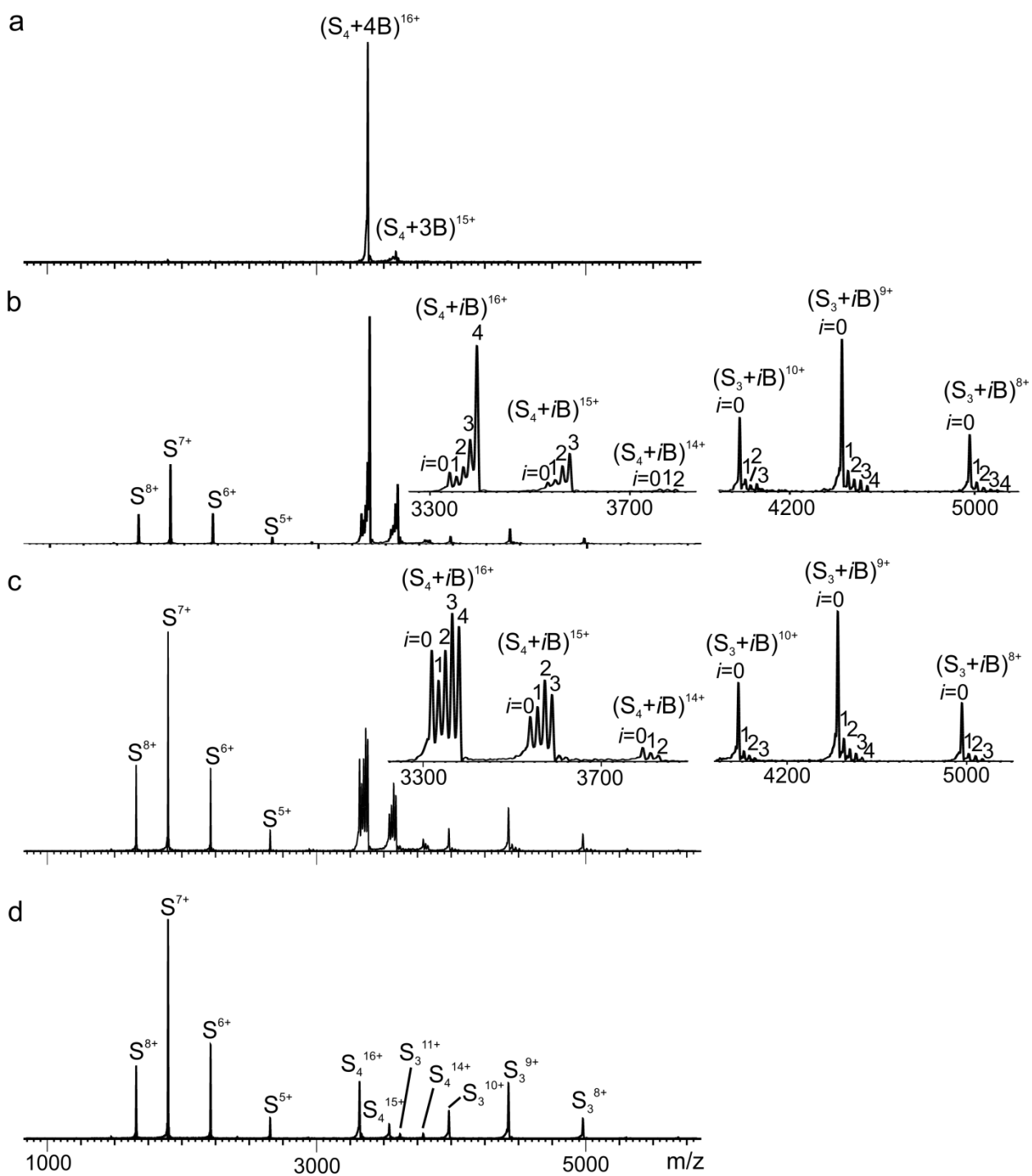
Figure S13. CID mass spectra in positive mode of the $(S_4 + 4B)^{16+}$ ion at a collision energy of (a) 3 V, (b) 24V, (c) 28 V and (d) 36 V.

51
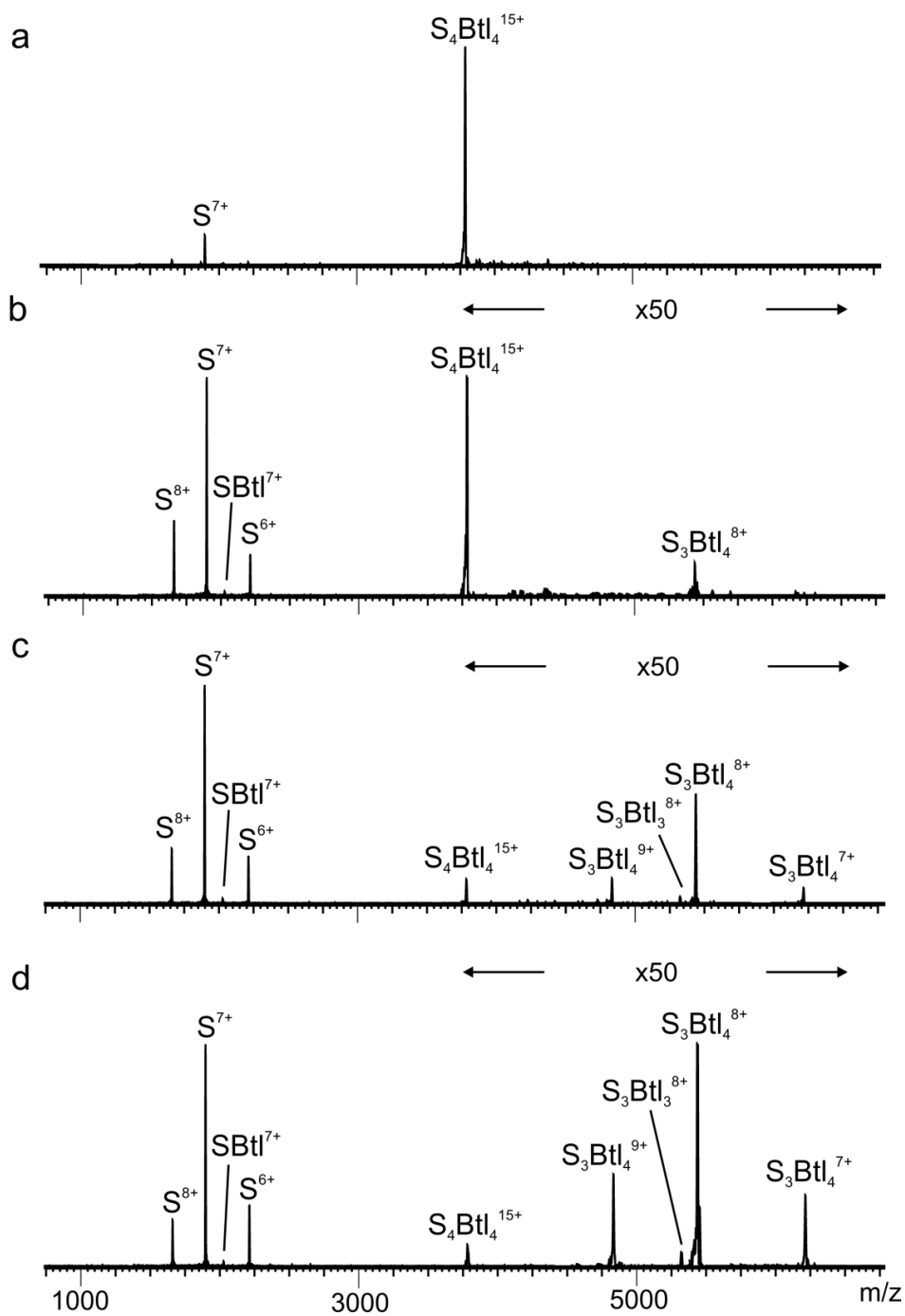
**Figure S14**. CID mass spectra in positive mode of the $(S4 + 4Btl)^{15+}$ ion at a collision energy of (a) 3 V, (b) 30 V, (c) 40 V, and (d) 50V. In (b), (c) and (d) the intensities in the m/z range 3700 - 6500 were magnified x50.
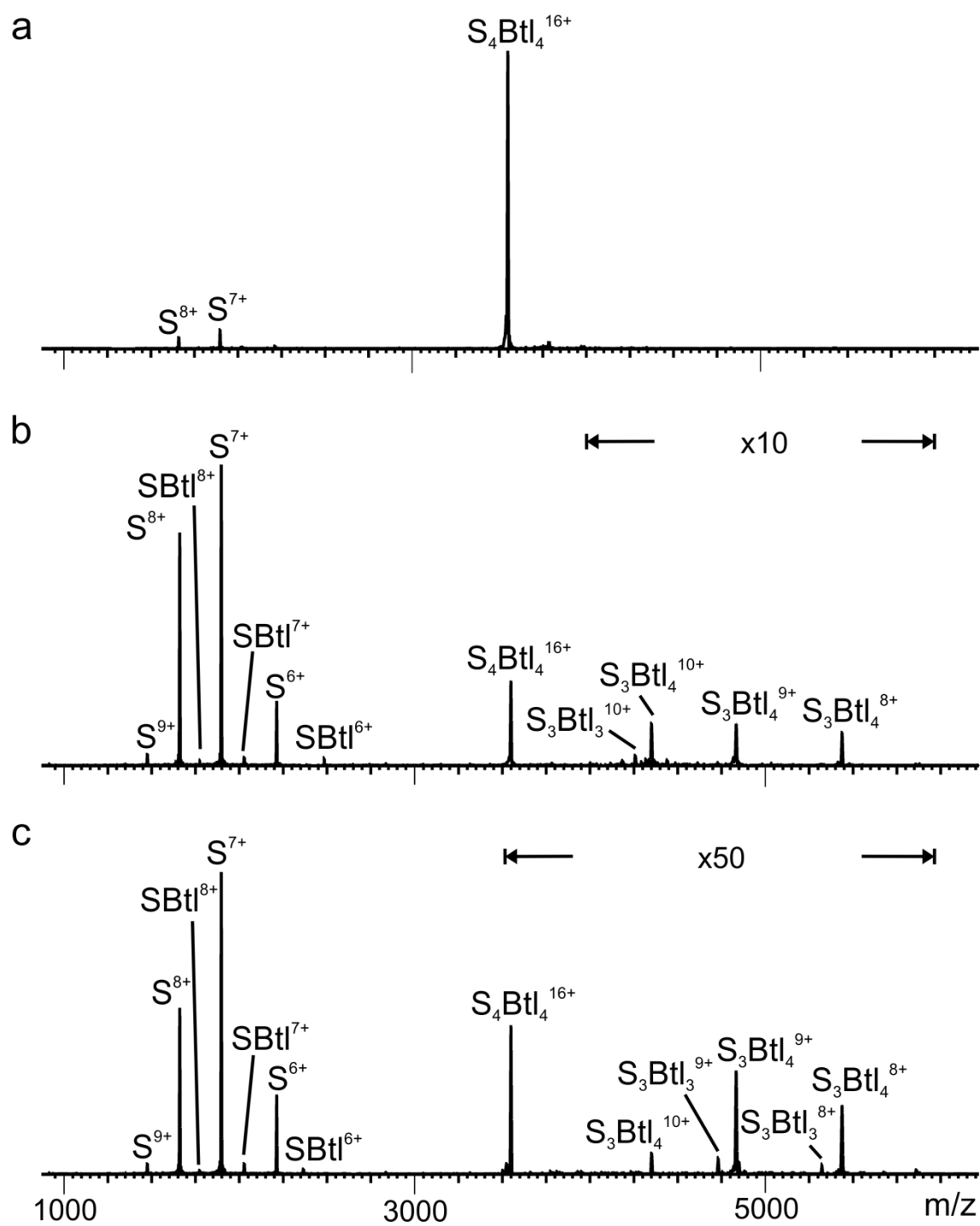
Figure S15. CID mass spectra in positive mode of the $(S_4 + 4Btl)^{16+}$ ion at a collision energy of (a) 3 V, (b) 25 V and (c) 40 V. In (b), the intensities in the m/z range 4000 - 6000 were magnified x10; in (c) the intensities in the m/z range 3500 - 6000 were magnified x50.
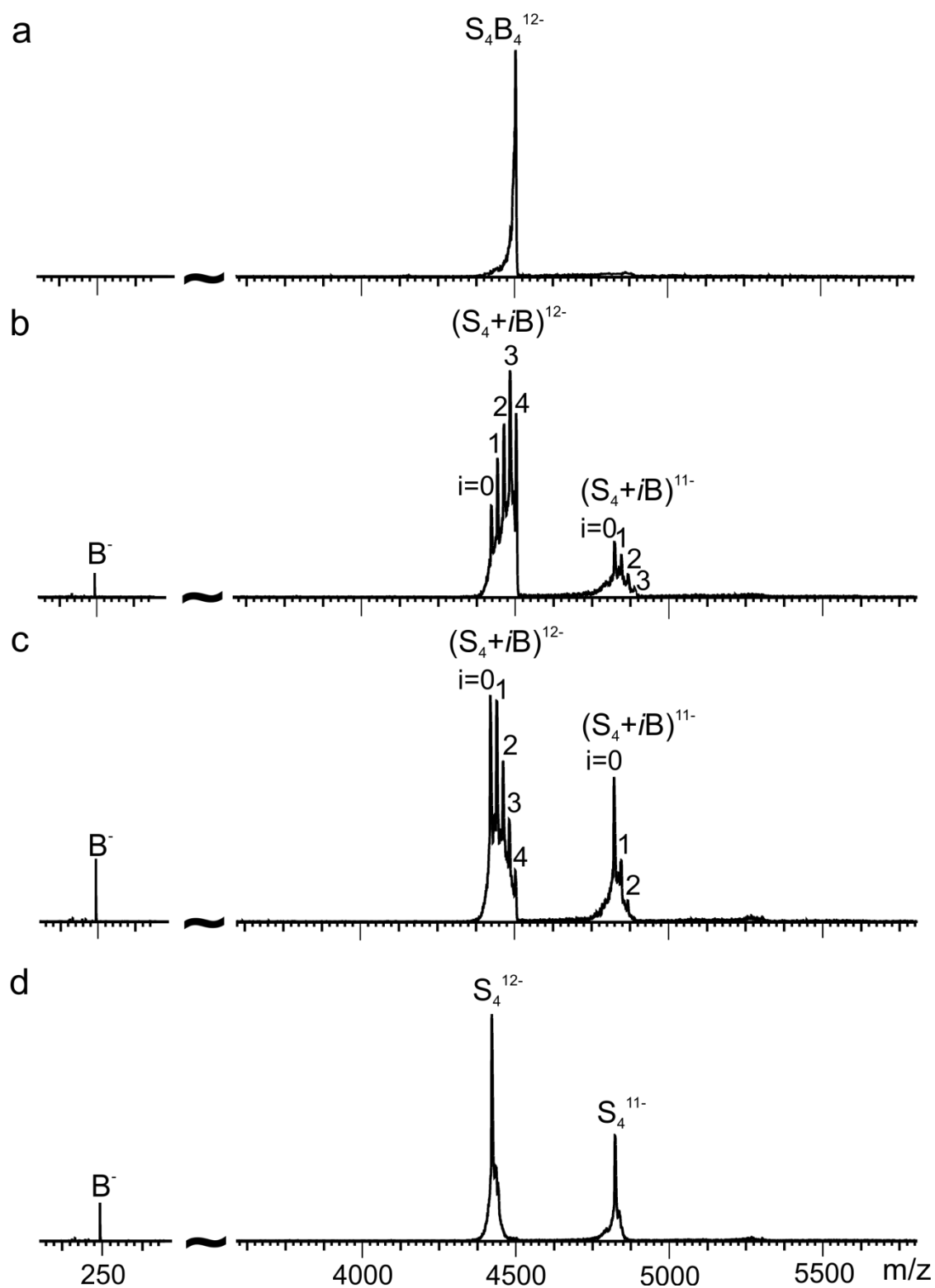
Figure S16. CID mass spectra in negative mode of the $(S_4 + 4B)^{12-}$ ion at a collision energy of (a) 3 V, (b) 28 V, (c) 32 V and (d) 40 V.
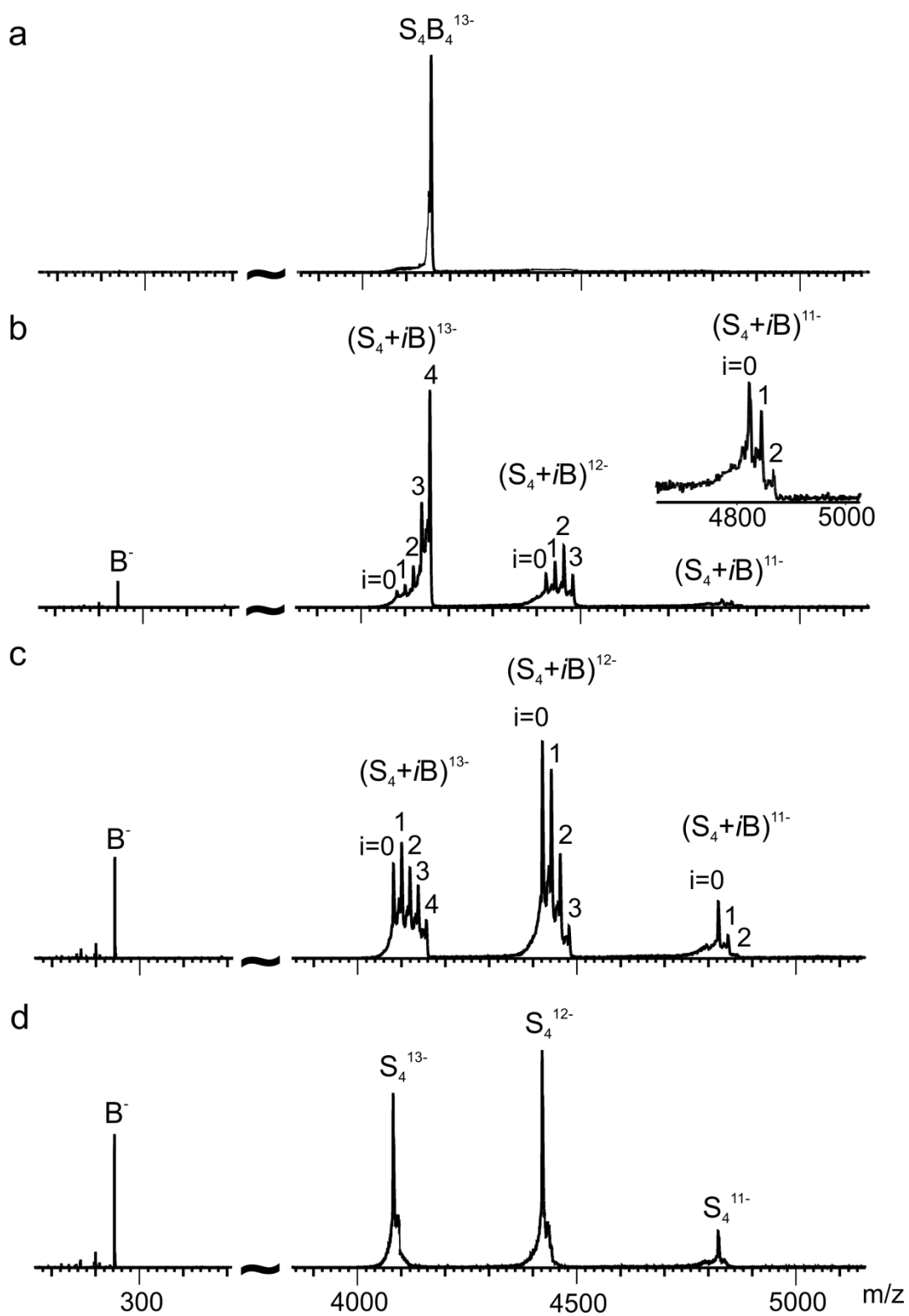
Figure S17. CID mass spectra in positive mode of the $(S_4 + 4B)^{13-}$ ion at a collision energy of (a) 3 V, (b) 20 V, (c) 26 V, and (d) 36 V.
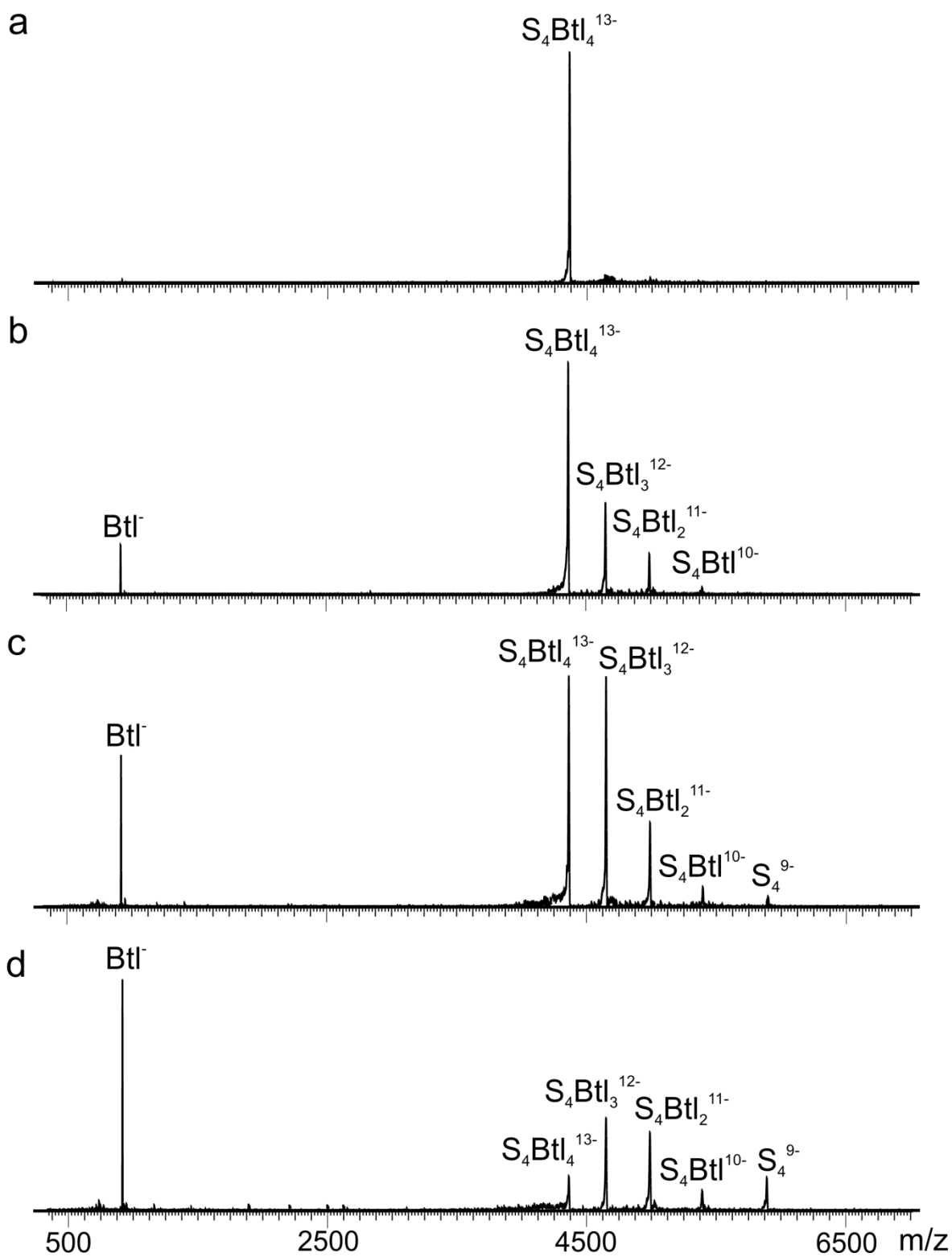
Figure S18. CID mass spectra in negative mode of the $(S_4 + 4Btl)^{13-}$ ion at a collision energy of (a) 3 V, (b) 20 V, (c) 40 V and (d) 60 V.
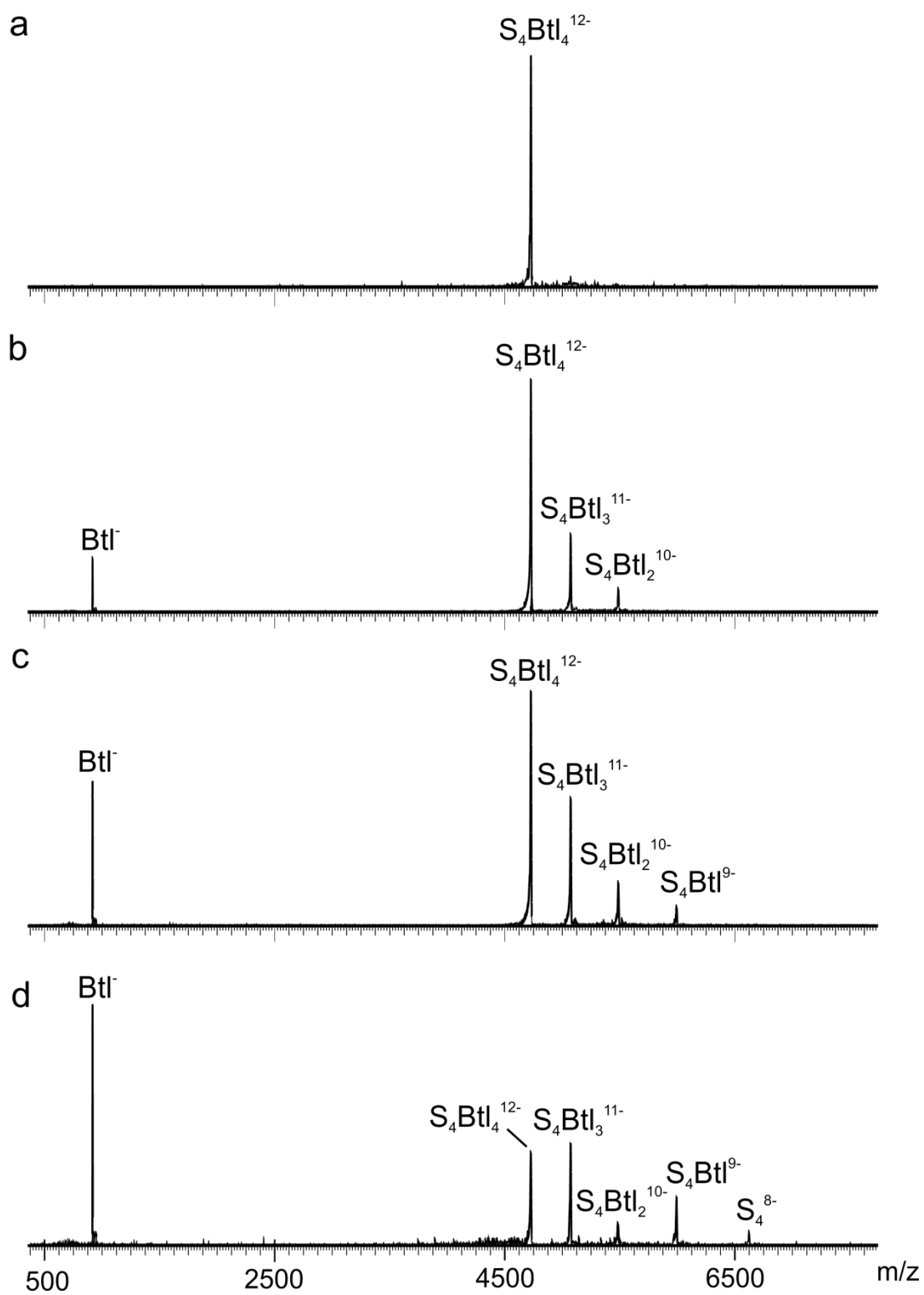
Figure S19. CID mass spectra in negative mode of the $(S_4 + 4Btl)^{12-}$ ion at a collision energy of (a) 3 V, (b) 20 V, (c) 40 V, and (d) 60V.
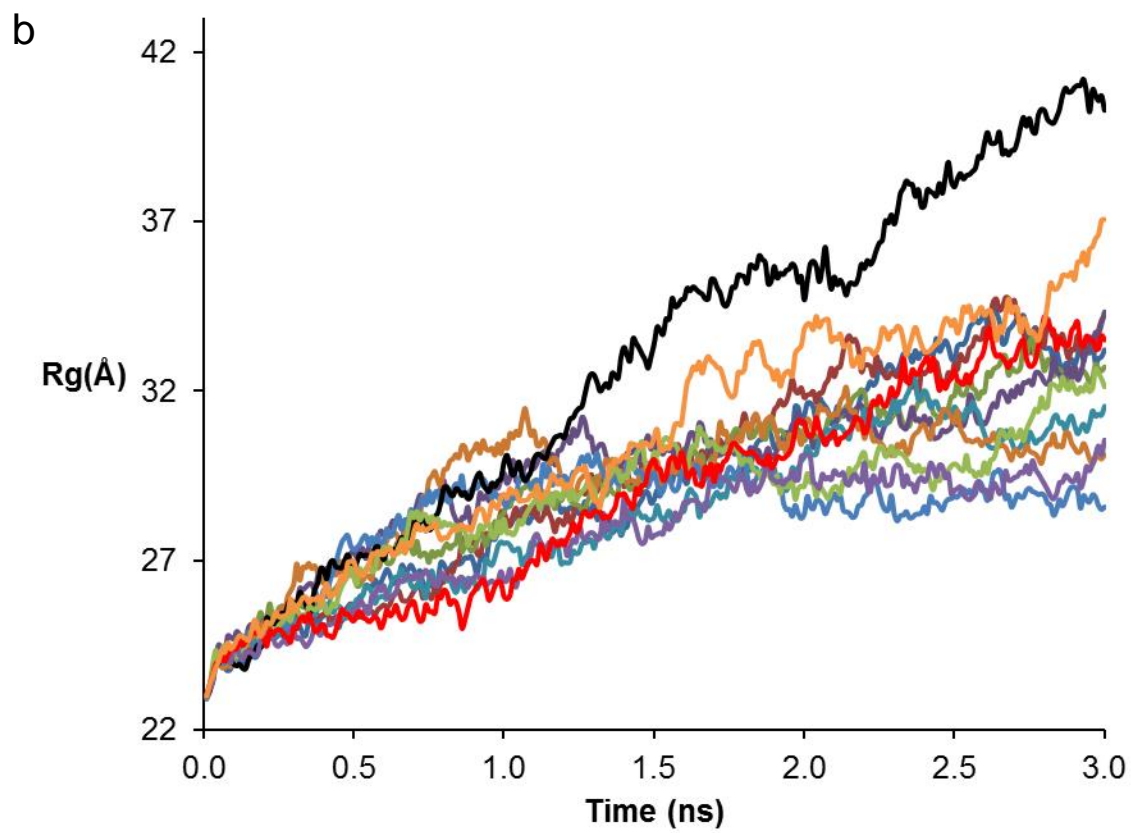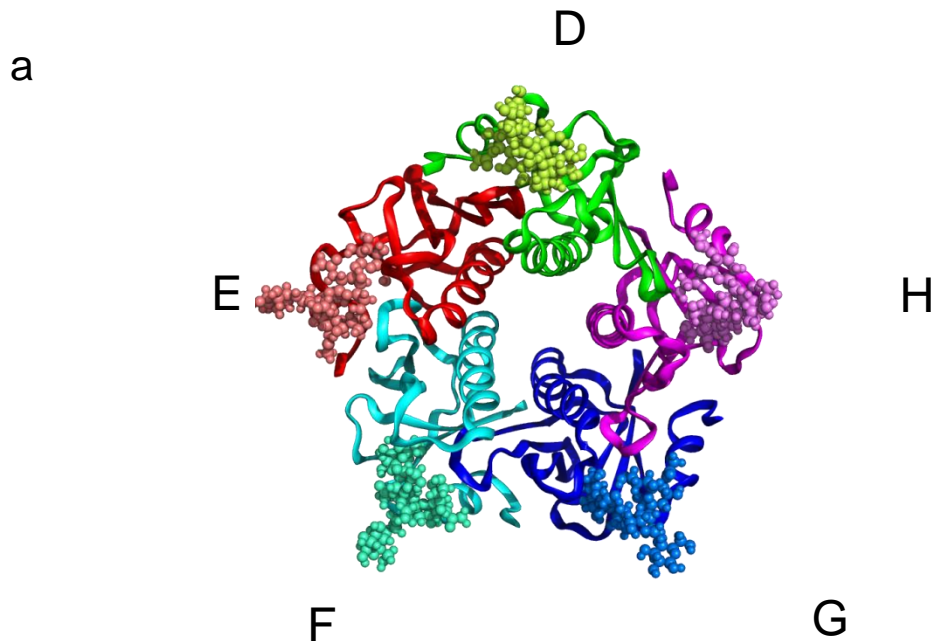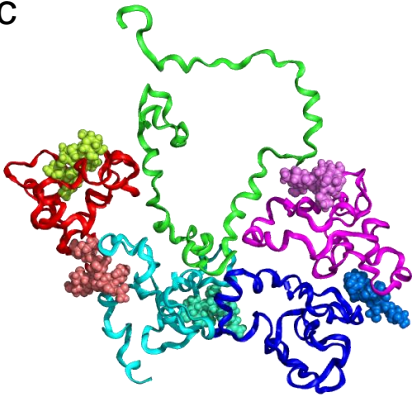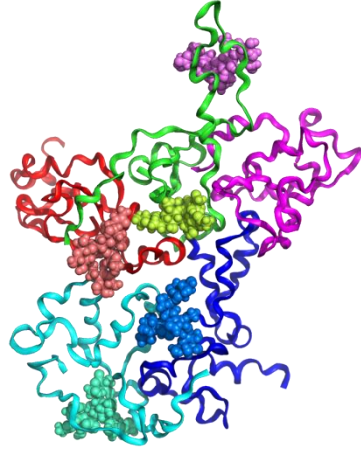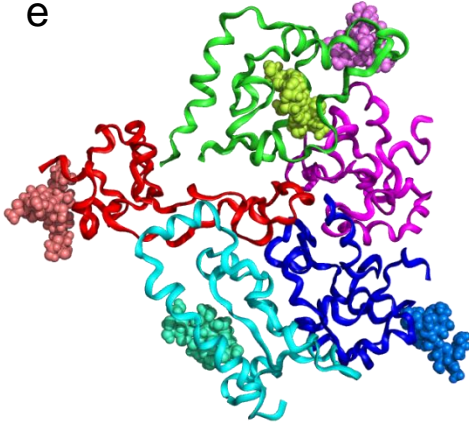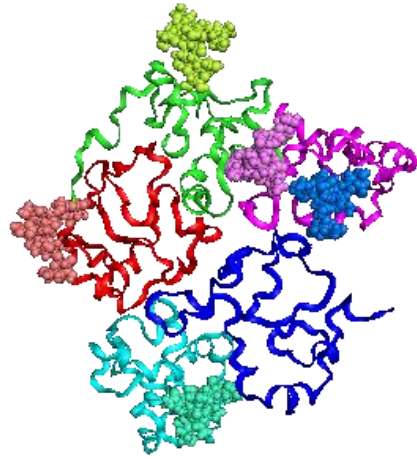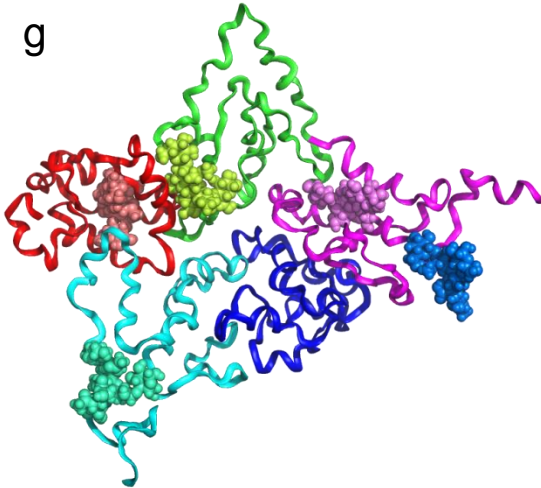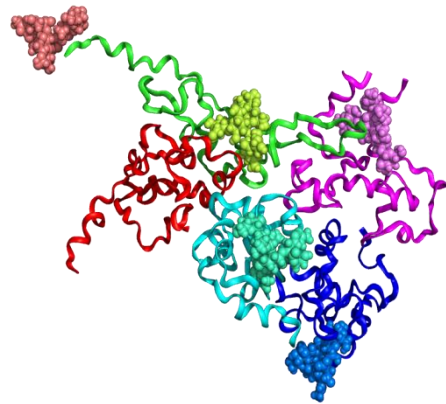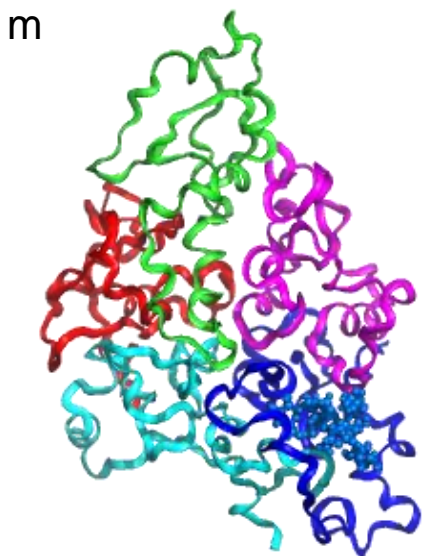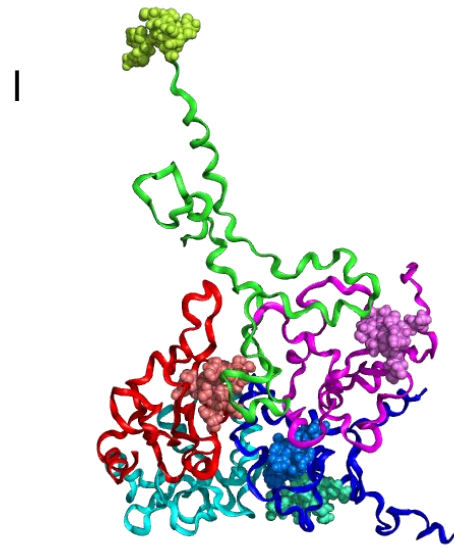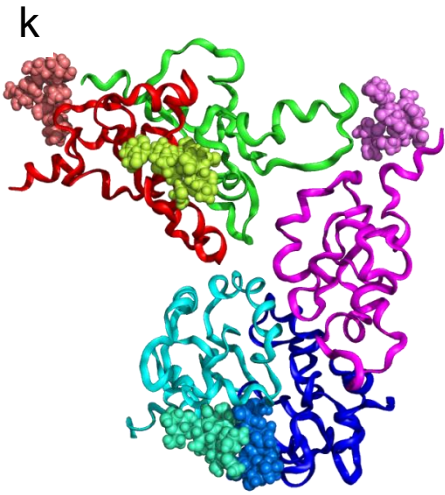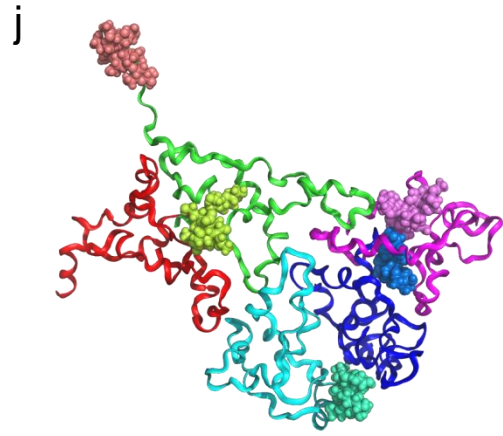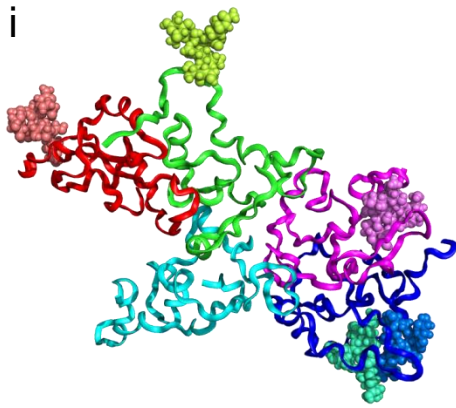
Figure S20. (a) Initial structure of the $(CTB_5 + 5GM1)^{15+}$ ion used for MD simulations. (b) Plots of Rg for 12 different charge configurations of $(CTB_5 + 5GM1)^{15+}$ ion calculated from the trajectories at 800 K. Charge configuration B15_1 (—), B15_2 (—), B15_3 (—), B15_4 (—), B15_5 (—), B15_6 (—), B15_7 (—), B15_8 (—), B15_9 (—), B15_10 (—), B15_11 (—), B15_12 (—). (c)-(m) Representative structures taken at ~1.5 ns for charge configurations: (c) B15_12, (d) B15_3, (e) B15_7, (f) B15_1, (g) B15_6, (h) B15_4, (i) B15_11, (j) B15_2, (k) B15_10, (l) B15_9 and (m) B9_1. Subunit D is shown in *green*, subunit E in *red*, subunit F in *light blue*, subunit G in *dark blue* and subunit H in *purple*. GM1 molecules are shown in the same colour as the subunit to which they are bound in the initial structure.